



HHS Public Access

Author manuscript

Biochim Biophys Acta Bioenerg. Author manuscript; available in PMC 2020 February 01.

Published in final edited form as:

Biochim Biophys Acta Bioenerg. 2019 February 01; 1860(2): 167–179. doi:10.1016/j.bbabi.2018.12.002.

The cytochrome *b* Lysine 329 residue is critical for ubihydroquinone oxidation and proton release at the Q_o site of bacterial cytochrome *bc*₁

Francesco Francia¹, Bahia Khalfaoui-Hassani^{2,#}, Pascal Lanciano², Francesco Musiani¹, Louis Noodleman³, Giovanni Venturoli^{1,4}, and Fevzi Daldal^{2,*}

¹Dipartimento di Farmacia e Biotecnologie, FaBiT, Università di Bologna, 40126 Bologna, Italy

²Department of Biology, University of Pennsylvania, Philadelphia, PA 19104, USA.

³The Scripps Research Institute, Department of Integrative Structural and Computational Biology, La Jolla CA 92037

⁴Consorzio Nazionale Interuniversitario per le Scienze Fisiche della Materia (CNISM), Dipartimento di Fisica, Università di Bologna, 40127 Bologna, Italy.

Abstract

The ubihydroquinone:cytochrome (cyt) *c* oxidoreductase (or cyt *bc*₁) is an important enzyme for photosynthesis and respiration. In bacteria like *Rhodobacter capsulatus*, this membrane complex has three subunits, the iron-sulfur protein (ISP) with its Fe₂S₂ cluster, cyt *c*₁ and cyt *b*, forming two catalytic domains, the Q_o (hydroquinone (QH₂) oxidation) and Q_i (quinone (Q) reduction) sites. At the Q_o site, the electron transfer pathways originating from QH₂ oxidation are known, but their associated proton release routes are less well defined. Earlier, we demonstrated that the His291 of cyt *b* is important for this latter process. In this work, using the bacterial cyt *bc*₁ and site directed mutagenesis, we show that Lys329 of cyt *b* is also critical for electron and proton transfer at the Q_o site. Of the mutants examined, Lys329Arg was photosynthesis proficient and had quasi-wild type cyt *bc*₁ activity. In contrast, the Lys329Ala and Lys329Asp were photosynthesis-impaired and contained defective but assembled cyt *bc*₁. In particular, the bifurcated electron transfer and associated proton(s) release reactions occurring during QH₂ oxidation were drastically impaired in Lys329Asp mutant. Furthermore, *in silico* docking studies showed that in this mutant the location and the H-bonding network around the Fe₂S₂ cluster of ISP on cyt *b* surface was

*Corresponding author: Fevzi Daldal fdaldal@sas.upenn.edu, Telephone: 215-898-4394.

#Present address: IPREM (Bâtiment IBEAS), UMR CNRS 5254, Université de Pau et des Pays de l'Adour, BP1155 Pau, France.

Author Contributions

FF, BK and PL designed, performed experiments and analyzed the data. FM and LN designed experiments and analyzed the data. All authors contributed to writing the manuscript. FD and GV managed the project, supervised the study, and wrote and edited the manuscript.

Conflict of Interest

The authors declare that the research was conducted in the absence of any commercial or financial relationships that could be construed as a potential conflict of interest.

Publisher's Disclaimer: This is a PDF file of an unedited manuscript that has been accepted for publication. As a service to our customers we are providing this early version of the manuscript. The manuscript will undergo copyediting, typesetting, and review of the resulting proof before it is published in its final citable form. Please note that during the production process errors may be discovered which could affect the content, and all legal disclaimers that apply to the journal pertain.

different than the wild type enzyme. Based on these experimental findings and theoretical considerations, we propose that the presence of a positive charge at position 329 of cyt *b* is critical for efficient electron transfer and proton release for QH₂ oxidation at the Q_o site of cyt *bc*₁.

Keywords

Cytochrome *bc*₁ complex; Complex III; Ubiquinol:cytochrome *c* oxidoreductase; Q_o site inactivation and proton release; Subunit interface; Bacterial photosynthesis and respiration

Introduction

The ubihydroquinone (QH₂): cytochrome (cyt) *c* oxidoreductase (cyt *bc*₁) of the purple bacterium *Rhodobacter capsulatus* has three catalytic subunits: the Rieske iron-sulfur protein (ISP) with its Fe₂S₂ cluster, cyt *b*, and cyt *c*₁ that represent a “catalytic core” common to all cyt *bc*₁ enzymes from diverse species [1]. The cyt *bc*₁ exploits the energetically favorable transfer of electrons from reduced quinone (QH₂) to oxidized cyt *c* to generate a transmembrane proton gradient, subsequently used for ATP biosynthesis. This membrane-integral enzyme operates following the modified *Q*-cycle mechanism [2]. Accordingly, the oxidation and reduction of QH₂ and oxidized quinone (Q) molecules take place at two catalytic sites, Q_{o(p)} and Q_{i(n)}, located on each side of the energy-transducing membrane. Following the oxidation of a QH₂ molecule at the Q_o site, two electrons are transferred to two different redox chains of cyt *bc*₁. The first electron is conveyed to a high potential redox chain, in which the ISP Fe₂S₂ cluster and the heme of cyt *c*₁ are reduced while two protons are released. The second electron from the QH₂ oxidation is received by a low potential chain, in which the cyt *b* hemes *b*_L and *b*_H are reduced sequentially. From the heme *b*_H of cyt *b*, this electron is conveyed to a Q molecule bound to the Q_i site, generating a semiquinone (SQ). A second turnover of cyt *bc*₁ fully completes the reduction of this SQ to a QH₂, which is then released from the Q_i site. With these successive reactions, the efficiency of cyt *bc*₁ in terms of proton translocation per oxidized QH₂ molecule increases twofold [3]. The above described *Q*-cycle mechanism postulates a sequential bifurcated electron transfer at the Q_o site, implying the formation of a SQ radical at Q_o. A so-called concerted (*versus* sequential) reaction mechanism, in which QH₂ at the Q_o site undergoes two simultaneous electron donations to the Fe₂S₂ cluster and heme *b*_L, has also been proposed (*e.g.*, [4]). This possibility is disfavored by the detection of electron paramagnetic resonance (EPR) signals attributed to SQ at the Q_o site, and in particular, by the observation of an EPR signal attributed to a spin-spin exchange of two unpaired electrons, one coming from SQ and the other from the reduced Fe₂S₂ cluster [5]. Related discussions could be found in [6].

In photosynthetic bacteria, the *Q*-cycle is common to both anoxygenic photosynthetic (Ps) and oxidative respiratory (Res) electron transfer pathways [7]. During the Ps growth, the QH₂ molecules arise from the activity of the photosynthetic reaction center (RC), which in turn receives electrons from the high potential redox chain of cyt *bc*₁ via soluble or membrane-attached electron carriers (like the cyt *c*₂ or cyt *c*_y) [8]. The cyclic electron transfer between the RC and cyt *bc*₁, energized by the photochemical activity of RC,

generates a proton gradient via the release to the periplasm of protons derived from QH₂ oxidation at the Q_o site and the uptake from the cytoplasm of protons coupled to Q reduction at the Q_i site of cyt *bc*₁ and at the RC. The electron and proton transfer reactions occurring at the Q_o site are tightly controlled in order to avoid the reactivity of the SQ intermediate formed during QH₂ oxidation [6, 9–11]. These SQ species represent a source of reactive oxygen species (ROS) whose amounts could be enhanced by decreased electron accepting abilities of the high potential redox chain of cyt *bc*₁ [12, 13].

Earlier studies have investigated the function of several cyt *b* residues located in the vicinity of the Q_o site in respect to QH₂ oxidation and catalytic turnover of cyt *bc*₁. Experimental evidence supports the important roles of cyt *b* residues Glu295 [14], Lys94 [15] and His291 [16] on the proton release pathway(s) to the periplasm. In addition, structural analyses indicated that Lys329 is among a set of cyt *b* residues that contributes to the docking surface for the extrinsic domain of ISP (ISP-ED) [17]. The cyt *b* ~ ISP-ED interaction surface is critical for correct positioning of the Fe₂S₂ cluster when the ISP-ED adopts the so called “*b*-position”, required for efficient electron transfer from the QH₂ bound at the Q_o site to the oxidized Fe₂S₂ of ISP. Upon reduction of the Fe₂S₂ cluster, a rapid movement (complete in < 100 μs [18, 19]) of the ISP-ED from the *b*-position to “*c*₁-position” occurs, allowing fast electron donation to the oxidized heme of cyt *c*₁. Studies showed that absence of the mobility of the ISP-ED [19–22], or perturbation of the surface loops at this region of cyt *b* via mutations or binding of Q_o site inhibitors [1, 23, 24], abolished efficient QH₂ oxidation. Specific mutations on the cyt *b* ~ ISP-ED interface tend to displace the ISP-ED from its native position at the Q_o site [25]. Indeed, the substitution with Gly [26] or Ala [17] of the highly conserved Lys329 of cyt *b* inhibited the cyt *bc*₁ activity. However, the basis of this inhibition, and in particular its role in the electron and proton transfer reactions during QH₂ oxidation has not been investigated in detail.

Theoretical considerations (*i.e.*, Density Functional Theory (DFT)-Continuum Electrostatic calculations) [27], and experimental redox potential *versus* pH (p*K*_a) measurements [28] suggested that electrostatic interactions of the Fe₂S₂ cluster with its surrounding environment are important [27–29]. Early on, we wondered how the electrostatic effects of a close-lying charged residue from the cyt *b* subunit would shift the p*K*_a's, and therefore the proton distributions, of the His ligands on the Fe₂S₂ cluster, particularly in the oxidized state. These external effects would add onto the electrostatic and dielectric effects internal (intrinsic) to the ISP-ED domain. The intrinsic effects, particularly their variations with sequence and structure, have been demonstrated by comparing the redox potential *versus* pH profiles of isolated ISP-ED's from different organisms [28], and by comparative DFT/dielectric based calculations and analyses [27, 29].

In the present work, we characterized the properties of *R. capsulatus* mutants where cyt *b* Lys329, located nearby the ISP-ED Fe₂S₂ cluster, was replaced by Arg, Asp and Ala residues. We found that while Lys329Arg had no significant effect on Q_o site catalysis, the Lys329Ala and Lys329Asp substitutions impaired both the Ps growth ability and the cyt *bc*₁ activity of these mutants. Time-resolved, light-activated spectroscopy showed that electron transfer along the low and high redox potential chains, as well as proton release from the Q_o site were inhibited, especially in the case of Lys329Asp mutation. Moreover, *in silico*

docking studies suggested that the presence of an Asp residue at position 329 of cyt *b* changed the equilibrium position of the ISP-ED, by increasing the Fe₂S₂ ~ Q_o site distance and perturbing the local H-bonding networks. Consequently, the transfer of the electrons and their coupled protons to the oxidized Fe₂S₂ cluster and its coordinating His residues of the ISP during QH₂ oxidation were impaired without affecting the mobility of the ISP-ED towards cyt *c*₁. Based on the overall experimental and computational data, theoretical considerations, and location of cyt *b* Lys329, we propose that a positive charge at this position nearby to the Fe₂S₂ cluster is critical for efficient transfer of the first electron and its coupled proton from QH₂ to oxidized Fe₂S₂ cluster of the ISP to initiate Q_o site catalysis of cyt *bc*₁.

Materials and Methods

1. Bacterial strains and growth conditions

Escherichia coli strains were grown at 37 °C on LB medium, supplemented with antibiotics (100 and 50 µg/mL of ampicillin (Amp) or kanamycin (Km), respectively), as needed. *Rhodobacter capsulatus* MT-RBC1 (*petABC*) and mutant strains were grown at 35 °C under respiratory (Res, chemoheterotrophic aerobic dark) or photosynthetic (Ps, anaerobic light) conditions in liquid or solid enriched medium (MPYE) or in Sistrom's minimal medium (MedA), supplemented with 10 µg/mL of Km antibiotic, as needed [30]. For Ps growth, completely filled culture vessels were used, and growth plates were placed in anaerobic jars with H₂ + CO₂ generating gas-packs (Becton, Dickinson Inc., MD) and incubated in temperature-controlled Percival light incubators [31].

2. Molecular genetic techniques

All strains and plasmids used in this work are listed in Table 1. Molecular genetic techniques were performed using standard procedures, as described earlier [32]. The plasmid pPETI-F [33] carrying the *petABC* operon encoding cyt *bc*₁ was used as a template, together with appropriate mutagenic primers for site-directed mutagenesis, to generate the Lys329 mutant derivatives (Table 2). This yielded the plasmids pBK13 (*petB*-K329R), pBK14 (*petB*-K329D), and pBK15 (*petB*-K329A), carrying the indicated substitutions at amino acid position 329 (*R. capsulatus* numbering) of cyt *b* (*petB*). The *R. capsulatus* replicative plasmid pMTSI carrying the *petABC* operon, was used to replace the wild type *petB* allele with appropriate *petB* K329 mutant variants [34]. The plasmids pMTSI and pPETI-F derivatives carrying the K329R, D or A substitutions, were digested with *Hind*III and *Eco*RI, and the wild type *petABC* operon of pMTSI was exchanged with its mutant derivatives carrying the *petB* K329 variants, yielding pBK23 (*petB*-K329R), pBK29 (*petB*-K329D) and pBK30 (*petB*-K329A). The *R. capsulatus* strains harboring pBK23, pBK29 and pBK30 were obtained by conjugation between appropriate *E. coli* HB101 derivatives used as donors (Table 1) and *R. capsulatus* MT-RBC1 carrying a complete chromosomal deletion of *petABC* operon (*i.e.*, cyt *bc*₁⁻ mutant) as a recipient, as described earlier [35].

3. Chromatophore preparation, SDS-PAGE, immunodetection, and steady-state cyt bc_1 activity

Chromatophores (or intracytoplasmic membrane vesicles) were prepared according to [36]. They were resuspended in 10 mM MOPS buffer, pH 7.00, kept at 4 °C, and used within a maximum of five days. Total protein concentrations were determined using the bicinchoninic acid assay, according to the supplier's recommendations (Sigma Inc.; procedure TPRO-562). For SDS-PAGE, prior to loading, 40 µg of total membrane proteins were solubilized in loading buffer to yield a final concentration of 62.5 mM Tris-HCl (pH 6.8), 2% SDS, 0.1 M dithiothreitol, 25% glycerol, and 0.01% bromophenol blue by incubation at room temperature for 10 min. After electrophoresis, the gels were either stained with Coomassie blue or electroblotted onto Immobilon-P polyvinylidene difluoride (PVDF) membranes (Millipore Inc., Billerica, MA) and probed with polyclonal antibodies against *R. capsulatus* cyt *b*. Antigen-antibody complex was visualized using horseradish peroxidase-conjugated anti-rabbit IgG secondary antibodies (GE, Healthcare Inc.), and signal detection used the Supersignal West Pico chemiluminescence substrate as recommended by the supplier (Thermo Fisher Inc.).

Steady-state cyt bc_1 activity was determined via the decylbenzohydroquinone (DBH₂):cyt *c* reductase activity. Reaction mixtures (2 mL) contained 50 mM sodium phosphate buffer (pH 7.4), 40 µM horse heart cyt *c*, 2 mM KCN, 0.1 g/L *n*-dodecyl-β D-maltoside (DDM), and 25 µg of total membrane proteins, as described earlier [35]. The reaction was started by adding to a stirred cuvette held at 25 °C 40 µM final concentration of DBH₂ (dissolved in dimethylsulfoxide), and time dependent cyt *c* reduction was monitored at 550 nm.

4. Optical redox and EPR spectroscopy, proton release kinetics, and related data analyses

Optical spectra were recorded using a Cary 60 spectrophotometer (Agilent Technologies Inc.). Optical spectra for the *c*- and *b*-type cyts were obtained using chromatophores (300 µg of total membrane protein per mL) oxidized with potassium ferricyanide and reduced with sodium ascorbate (for *c*-type hemes) or sodium dithionite (for *b*- and *c*-type hemes) as appropriate.

Electron paramagnetic resonance (EPR) characterization of *R. capsulatus* strains carrying the cyt *b* Lys329Ala, Asp or Arg substitutions was carried out as done earlier [20]. Membranes were prepared as above and reduced with ascorbate in the absence and presence of the cyt bc_1 inhibitor famoxadone. The EPR spectra were recorded as indicated in the figure legends.

Kinetics of flash-induced carotenoid band shift, as well as of redox changes of cyt *c*, cyt *b*, and of the RC primary electron donor (P) were recorded as described previously [16], except that the redox mediators phenazine methosulfate and phenazine ethosulfate were omitted, as needed. Detection of flash-induced Neutral Red (NR) absorption transients was described in [16, 37]. The cyt bc_1 content of chromatophores was determined based on the dithionite-reduced *minus* ascorbate-reduced spectra as described earlier [16]. For measurements of proton release kinetics using the pH indicator dye NR, chromatophores were further washed

twice with 2mg/mL BSA buffer, pH 7.5, and used the same day. The total bacteriochlorophyll concentration ([BChl]) of chromatophores was estimated upon extraction by organic solvents, as described in [38]. All data processing were carried out as earlier [16].

5. Docking analyses

The higher resolution three dimensional structure of cyt *bc*₁ from *Rhodobacter sphaeroides* (PDB code: 2QJY) [39] (instead of that from *R. capsulatus*) was used for docking studies. Specifically, the structure of the ISP-ED (residues 50–187) was docked onto wild type and Lys329Asp mutant cyt *b* using the data-driven docking program High Ambiguity Driven biomolecular DOCKing (Haddock) 2.2 [40, 41]. Haddock implements a knowledge-based approach that uses biochemical and biophysical interactions data to drive the docking process. The calculations were guided by defining the most conserved residues at the ISP-ED ~ cyt *b* interface as “active” in the protein-protein interaction. The docking algorithm rewards the complexes that have these active residues on the interaction interface. The solvent accessible residues that are found on the surface of the partner proteins and in contact with active residues were included in the calculation as “passive” residues. Table 3 lists the complete set of active and passive residues used in the docking calculations. Each docking calculation involved three stages: first, a rigid body energy minimization was carried out and 1000 structures were calculated; second, based on the intermolecular energy the 200 best solutions were used for a semi-flexible simulated annealing step; and third, a final explicit water refinement of the same 200 best solutions was carried out. The 200 refined models were clustered using a cutoff of 7.5 Å, based on the pairwise backbone root mean square deviation (RMSD) matrix and a minimal cluster population of four binding poses. Residue conservation was evaluated by using the ConSurf 2016 web server [42]. The structural model of cyt *b* Lys329Asp mutant was generated using the Modeller 9.19 software [43, 44]. The force field parameters for heme *b* and Fe₂S₂ cluster were already included in the Haddock suite. Stigmatellin was parameterized using the PRODRG server [45], and the atomic charges were calculated by adopting the RESP procedure on the HF/6–31G(d) optimized structure, calculated using the NWChem software [46]. The molecular graphics images were produced using the UCSF Chimera package [47].

Results

1- Rationale for choosing cyt *b* Lys329 residue to probe its role in Q_o site catalysis

Earlier theoretical considerations [27] and experimental data [28] indicated that a positively charged residue near the Fe₂S₂ cluster of the ISP, which is an anion under physiological redox and protonation states (the overall cluster charge is zero only when the oxidized state is at acidic pH, where pH is significantly less than the pK_a's on the His ligands) might be important to drive the proton coupled electron transfer to initiate QH₂ oxidation at the Q_o site [27, 29]. The conserved charged surface residues of cyt *b* that are located near the Fe₂S₂ cluster when the ISP-ED is docked to the Q_o site were examined for their ability to interact electrostatically with the oxidized Fe₂S₂. This analysis led to the highly conserved cyt *b* Lys329, which could play an important role with Q_o site catalysis when mutated [17, 26]. We therefore targeted this residue using site-directed mutagenesis, and substituted it with a

positively charged (Arg), a neutral (Ala), and a negatively charged (Asp) amino acid residue, and examined their properties.

2- Effect of the cyt b Lys329 mutations on *R. capsulatus* Ps growth

The purple non sulfur bacterium *R. capsulatus* requires an active cyt bc_1 for Ps growth, but its Res growth is cyt bc_1 -independent, as it can also be carried out via its alternate quinol oxidase [48]. The Ps growth abilities of mutants carrying the cyt *b* Lys329Arg, Ala and Asp substitutions were compared with a “wild type” *R. capsulatus* strain carrying a native cyt bc_1 (encoded by *petABC* operon) on the plasmid pMTS1 harbored by a mutant lacking cyt bc_1 (pMTS1/MT-RBC1) [23]. On enriched medium (*i.e.*, unbuffered MPYE, pH initially adjusted to 7.0), all strains were able to grow by Res, but only the wild type and Lys329Arg and not the Lys329Ala and Lys329Asp strains grew by Ps. This phenotype indicated that the cyt bc_1 of the latter two mutants were defective, but their Ps growth improved when a pH-buffered minimal medium (*e.g.*, MedA, buffered with 100 mM phosphate pH, 7.0) was used instead of enriched medium (Fig. 1).

3- The cyt bc_1 contents of cyt b Lys329 mutants

In order to assess semi-quantitatively the effects of the Lys329Arg, Ala and Asp mutations on the assembly and amount of cyt bc_1 in various mutants, SDS-PAGE, immunoblot, optical redox difference (Fig. 2), and EPR (Fig. 3) spectroscopy were used. The strains containing pMTS1 and its mutant derivatives overproduced cyt bc_1 , rendering visible similar amounts of the ISP, cyt *b* and cyt c_1 subunits in membranes separated by Coomassie blue stained SDS-PAGE (Fig. 2A). Immunoblot analyses using antibodies against cyt *b* showed that all mutants contained similar amounts of this subunit (Fig. 2B), and dithionite-reduced *minus* ferricyanide-oxidized optical spectra indicated that the *b*-type (560 nm peak) and *c*-type (550 nm peak) heme contents of membranes of all mutants (except MT-RBC1 lacking cyt bc_1) were comparable (Fig. 2C). In addition, EPR spectroscopy of appropriate samples showed that the g_y transitions corresponding to the reduced Fe_2S_2 cluster of the ISP were comparable in all strains (Fig. 3). Thus, mutating Lys329 of cyt *b* had no drastic effect on the *in vivo* amount or subunit and cofactor assembly of cyt bc_1 . We note that the $g_x = 1.80$ transitions of the reduced Fe_2S_2 cluster of the ISP were modified in the Lys329Ala and Lys329Asp mutants as compared with the wild type and the Lys329Arg mutant, indicating perturbations between the Fe_2S_2 cluster and the quinone residing at the Q_o site. Similarly, the responses of the latter mutants to the cyt bc_1 inhibitor famoxadone were different than the wild type and the Lys329Arg mutant, as indicated by their $g_x = 1.78$ transitions (Fig. 3).

4. Steady-state cyt bc_1 activities of cyt b Lys329 mutants

Next, the steady-state cyt bc_1 activities of Lys329 mutants were measured using DBH_2 :cyt *c* reduction assays (Materials and Methods). Membranes of *R. capsulatus* wild type strain (pMTS1/MT-RBC1) exhibited an activity of 1.19 μ moles of cyt *c* reduced/min/mg of total membrane proteins (referred to as 100%). This activity was decreased to 13.5 % upon addition of 10 μ M of antimycin, which is a specific Q_1 site inhibitor, confirming that a large fraction of the measured activity indeed corresponded to cyt bc_1 . As expected, membranes from a strain lacking cyt bc_1 (MT-RBC1) showed ~ 2% of wild type activity as cyt bc_1 -independent background. On the other hand, the Lys329Arg, Lys329Ala and Lys329Asp

mutants had lower antimycin-sensitive cyt bc_1 activities, corresponding to ~ 85%, 33% and 11% of that of a wild type (pMTS1/MT-RBC1) strain, respectively, in line with their Ps growth abilities (Table 4). Thus, the Lys329Ala and Lys329Asp substitutions rendered the cyt bc_1 significantly defective, and required analysis of their electron and proton transfer activities. We note that in all cases the antimycin-insensitive residual activities should not be equated with superoxide-mediated cyt c reduction as this latter activity was not determined.

5. Effects of the cyt b Lys329 mutations on flash-induced carotenoid band shift kinetics

Using dark-adapted chromatophore vesicles, the time dependence of the membrane potential (ψ) can be monitored using the carotenoids electrochromic signal (CS) upon induction of the RC charge separation by a short actinic flash of light [49] (Fig. 4). The first two phases of the CS kinetics, completed in a few μ sec, separation inside the RC and the oxidation of the electron carrier cyts c by the photo-oxidized RC. A third, slower phase of CS (phase III), completed in the ms time scale, reflects the electrogenic events that occur within the cyt bc_1 . Originally, the phase III of CS has been attributed to the electrogenicity of the movement along the low potential chain of electrons originating from QH_2 oxidation at the Q_o and subsequent Q reduction at the Q_i sites [50]. In the presence of antimycin, electron transfer from heme b_H to Q residing at Q_i site is blocked, allowing further resolution of the phase III into antimycin-sensitive, and antimycin-insensitive but myxothiazol-sensitive phases attributed to heme b_H oxidation and reduction, respectively [51]. Addition of the Q_o site inhibitor myxothiazol prevents oxidation of QH_2 and reduction of heme b_L . A subsequent alternative interpretation proposed that phase III of CS might reflect predominantly the electrogenic uptake/release of protons linked to the oxidation of heme b_H and to the reduction of cyt c_1 [52]. In any event, myxothiazol completely eliminates phase III to leave only the portion of CS corresponding to the electrogenic events due to RC photo-oxidation. The latter amplitude observed in the presence of myxothiazol could be used to normalize the CS signals between samples, as it is directly proportional to the charges transferred across the photo-oxidized RC. Such normalized CS signals for various mutants are shown in Fig. 4. In wild type membranes, a slower phase III corresponding to cyt bc_1 activity was clearly seen (black trace). In the mutants, the amplitude and initial rate of this phase III decreased progressively from Lys329Arg (red trace) to Lys329Ala (green trace) mutations. The Lys329Asp (dark blue trace) mutation abolished almost completely the phase III of CS (Fig. 4, note the break in the time axis), establishing that the cyt bc_1 associated electrogenic events were perturbed in the mutants.

The effect of Lys329 substitutions on the kinetics of the cyt bc_1 electrogenic events are better appreciated using the differential signals obtained by subtracting the CS signals obtained after addition of antimycin (*i.e.*, antimycin-sensitive phase III) from those recorded using the uninhibited chromatophores (Fig. 5). For each mutant, traces have been normalized to the maximal absorbance change reached, and the data showed that the rate change of the antimycin-sensitive phase III was negligible in the case of Lys329Arg (red trace). In contrast, this rate change was clearly visible with Lys329Ala (green trace), and became well pronounced with Lys329Asp (dark blue trace) mutations.

6. Effects of the cyt b Lys329 mutations on flash-induced cyt c re-reduction kinetics

Reduction of cyt *c* and cyt *b* hemes and effects of specific inhibitors on light-induced turnover kinetics allows dissection of the electron transfer steps internal to cyt *bc*₁. In dark adapted chromatophores redox poised at an E_h of ~ 110 mV, the high potential redox chain cofactors Fe₂S₂ and heme *c*₁ are reduced, whereas the low potential redox chain cofactors hemes *b*_L and *b*_H are oxidized. Upon excitation by a flash of light, the photo-oxidized primary electron donor of the RC is quickly reduced via the electron carrier cyts *c* (*c*₂ and *c*_γ in *R. capsulatus*) that in turn rapidly transfer the oxidizing equivalents to cyt *c*₁ to activate the cyt *bc*₁ turnover. The oxidized cyt *c*₁ is re-reduced by the Fe₂S₂ cluster of the ISP-ED, which receives an electron from the oxidation of QH₂ molecule at the Q_o site, yielding a transient SQ. The transfer of electrons from the Q_o site to cyt *c*₁ via the Fe₂S₂ center requires a large-scale movement of the ISP-ED, which is essential for cyt *bc*₁ catalysis. In wild type chromatophores, the flash-induced cyt *c* re-reduction kinetics under uninhibited conditions (Fig. 6, black trace in panel WT) reflected the sequence of the redox events described above. A fast, unresolved oxidation of cyts *c* was followed by a re-reduction phase in the ms time scale via electrons shuttled by the ISP-ED from the Q_o site. Under our conditions, addition of antimycin barely affected (green trace), whereas that of myxothiazol (blue trace) clearly inhibited, these cyt *c* re-reduction kinetics by impeding the Q_o site catalysis. In addition, the flash-induced extent of total cyts *c* oxidation increased by adding stigmatellin (red trace), which trapped the ISP-ED at cyt *b* surface to block its large-scale movement required to bring the reduced Fe₂S₂ cluster near cyt *c*₁ heme for fast electron transfer. In the presence of stigmatellin, the electron residing in the ISP-ED (at the E_h of ~ 100 mV used here) is blocked, revealing complete extent of oxidized cyts *c*. The data indicated that all Lys329 mutants were sensitive to myxothiazol (blue traces) and to stigmatellin (red traces) (Fig. 6), but in the absence of any inhibitor the re-reduction of the flash-oxidized cyts *c* was weakly and strongly slowed down in the Lys329Ala and Lys329Asp mutants, respectively (Fig. 6, panel KA and KD, black traces). In particular, the slow electron delivery to oxidized cyt *c*₁ in the Lys329Asp mutation was well visualized when the cyt *c* kinetics obtained in the absence of inhibitor were overlapped (Fig. 7A). In the mutants, the cyt *c* re-reduction rates were not due to impaired movement of the ISP-ED as the amplitude of cyt *c* oxidation seen in the presence of myxothiazol increased clearly upon addition of stigmatellin [19, 20]. This finding was further supported quantitatively in Fig. 7B, by subtracting the cyt *c* kinetics traces recorded after addition of stigmatellin (Fig. 6, red traces) from those obtained in the presence of antimycin plus myxothiazol (Fig. 6, blue traces), establishing that in all Lys329 mutants the large-scale movement of the ISP-ED was unperturbed. Thus, the slowing down of the electron residing on the pre-reduced Fe₂S₂ center to cyt *c*₁ reflected slow Q_o site catalysis.

7. Effects of the cyt b Lys329 mutations on flash-induced cyt b reduction kinetics

Delivery of the second electron originating from QH₂ oxidation at the Q_o site to the low potential cyt *b* chain can be monitored by following the reduction of heme *b*_H in the presence of antimycin, which impedes electron transfer from heme *b*_H to Q molecule at the Q_i site. Thus, flashinduced cyt *b* reduction kinetics in wild type and mutant stains were examined (Fig. 8). At an E_h of ~ 115 mV, the reduction rate of heme *b*_H approaches its maximum, due to the large amount of QH₂ present in the Q pool that can react at the Q_o site,

and the pre-oxidation of the low potential chain hemes *b*. The data showed that cyt b_H reduction rate was strongly impaired in the Lys329Asp substitutions, in line with the cyt bc_1 associated phase III of CS (Figs. 4 and 5) and cyt *c* re-reduction kinetics (Figs 6 and 7A). Since the delivery of the first electron from QH₂ oxidized at the Q_o site to the high-potential chain of cyt bc_1 is a prerequisite for reduction of the low potential chain by the second electron, the observed effects on cyt b_H reduction kinetics confirmed the perturbed cyt *c* re-reduction kinetics seen in the mutants. Thus, the presence of a negatively charged residue at the position 329 of cyt *b* was inhibitory to the reduction of cyt b_H .

8. Flash-induced proton release in the cyt *b* Lys329 mutants

R. capsulatus cells broken up using a French press yield chromatophore membranes that are inverted vesicles (Materials and Methods). Flash activation of cyt bc_1 catalysis induces transient acidification of the internal lumen of these vesicles due to proton release coupled to QH₂ oxidation at the Q_o site. The decrease of pH, reflecting this proton release, can be monitored by following the flash-induced absorption changes at 546 nm of the amphiphilic pH indicator dye NR. Measurements were performed on chromatophores incubated with 13 μM NR, 1 mM Na-ascorbate and the redox mediator 2,3,5,6-tetramethyl-*p*-phenylenediamine (3,6 diaminodurene or DAD) in order to obtain an E_h comparable to that employed when examining electron transfer kinetics [16]. Absorption changes that reflect only the proton release kinetics from the Q_o site were obtained by subtracting the kinetics obtained in the presence of antimycin A and myxothiazol from those recorded in the absence of inhibitor, and the absorbance increase seen at 546 nm reflected the NR detected lumen acidification for chromatophores from the wild type and Lys329 mutants (Fig. 9). The half times of proton release kinetics were essentially coincident in the wild type and in the Lys329Arg mutant, while slightly slower and strongly retarded kinetics were seen with the Lys329Ala and Lys329Asp mutants, respectively. Thus, the kinetics of proton release coupled to QH₂ oxidation at the Q_o site were affected especially by the Asp substitution, again in line with the cyt *c* and cyt *b* electron transfer kinetics and CS associated with mutant cyt bc_1 . We concluded that the loss of the positive charge at position 329 of cyt *b* to a neutral one inhibited partially, whereas its substitution with a negative charge abolished drastically the Q_o site catalysis of cyt bc_1 .

9. Docking studies

The structural effects induced by the cyt *b* Lys329Asp mutation were further examined *in silico* using molecular recognition (docking) calculations (Materials and Methods). Since the available *R. capsulatus* cyt bc_1 (PDB code: 1ZRT) structure [53] was not suitable for these calculations due to its low (3.5 Å) resolution and other structural parameters ($R_{Free} = 0.358$, 21% of Ramachandran outliers, 22% of side-chain outliers), the higher resolution structure of *R. sphaeroides* [39] with its better structural parameters (PDB code: 2QJY, resolution: 2.4 Å, $R_{Free} = 0.251$, 1% of Ramachandran outliers, 4% of side-chain outliers) was chosen. This choice was acceptable as the *R. capsulatus* and *R. sphaeroides* cyt bc_1 share very high homology (84%, 61%, and 75% sequence identity for cyt *b*, cyt c_1 , and ISP subunit, respectively).

For the docking calculations, first a benchmark calculation was run to obtain *in silico* a wild type cyt *b* ~ ISP-ED complex from *R. sphaeroides*. Then, a second docking calculation was performed in which the structure of cyt *b* Lys329Asp was modeled *in silico* using the same modelling procedure. In both cases the transmembrane portion of ISP and cyt *c*₁ were excluded to simplify the calculations, which was justified as the ISP-ED large-scale movement was unaffected by the cyt *b* Lys329Asp mutation (Figs 6 and 7). Both docking calculations were run by adopting a knowledge-based docking approach, and guiding molecular recognition through the use of the most conserved residues of the ISP-ED and cyt *b* (Table 3), located on their interaction surface in the proximity of the Q_o site and the Fe₂S₂ cluster.

The 200 structures resulting from the first benchmark docking were clustered based on the RMSD of the protein backbone, yielding one cluster containing 181 and the other 7 structures (the remaining 12 structures were not assigned to any cluster). A representative structure from the most populated cluster is depicted in Fig. 10A and B. The general molecular geometry of the wild type cyt *b* ~ ISP-ED complex is in agreement with that found in the crystal structure. Superimposition of the C α atoms of cyt *b* from the calculated best structure with those of the crystal structure, yielded a C α RMSD for ISP-ED of 2.08 Å. This deviation decreased to 0.94 Å when only the residues located in the vicinity of the Fe₂S₂ cluster (128–137 and 148–155, *R. sphaeroides* numbering) were considered. The data showed that this region of cyt *bc*₁ involved in the electron transfer was modeled with good accuracy. Both in the crystal structure and in the wild type model complex, the cyt *b* Lys329 side chain NH₂ group formed an H-bond with the backbone oxygen of ISP-ED His131 (corresponding to His135 in *R. capsulatus* numbering), which is one of the two His ligands of the Fe₂S₂ cluster [17].

The good agreement seen between the model obtained by the benchmark calculation and the available crystal structure allowed us to run a second round of docking calculations to assess the effects induced by the cyt *b* Lys329Asp mutation. As with the benchmark calculations, the 200 binding structures that resulted from the second docking calculations were clustered, and yielded four clusters populated by 165, 16, 7, and 4 model structures of the mutated cyt *b* ~ ISP-ED complex. A smaller number (2 *vs* 4) of clusters, and a larger number (181 *vs* 165) of structures in the most populated clusters were obtained with the wild type *versus* the mutated complexes, suggesting that formation of the mutated protein complex was slightly less favored than the wild type complex.

In the mutated complex case also, the most representative structure from the most populated cluster is depicted in Fig. 10A and C. As in the previous case, the overall molecular geometry of the mutant cyt *b* ~ ISP-ED complex was in excellent agreement with the wild type complex found in the crystal structure. In this case, the C α RMSD for ISP-ED was 1.86 Å, which decreased to 1.28 Å when only the residues in the vicinity of the Fe₂S₂ cluster were considered. The data suggested that the overall model of the mutant complex was more similar to the wild type crystal structure than the similarly modeled wild type complex (1.86 Å *versus* 2.08 Å, respectively). However, the region involved in electron transfer was modeled with a higher accuracy in the case of the wild type complex (0.94 *versus* 1.28 Å), which was confirmed by the RMSD of the Fe₂S₂ cluster (0.76 and 1.08 Å for the wild-type

and the mutant complexes, respectively). Indeed, the distance between the stigmatellin and the center of the Fe_2S_2 cluster in the wild type complex was shortened by $\sim 0.20 \text{ \AA}$, whereas it was lengthened by 0.71 \AA in the case of the mutant complex. The comparisons of the distances between stigmatellin and the Fe_2S_2 liganding residues (*i.e.*, ISP-ED His131, Cys149 and His152, corresponding to His135, Cys153 and His156 in *R. capsulatus* numbering) also showed a similar trend. Furthermore, in the mutant complex, the cyt *b* Asp329 residue was found at a H-bonding distance from the side chain of ISP-ED His131 (Fig. 10C), indicating that the formation of this bond could shift away the position of the Fe_2S_2 cluster, and consequently that of His152 (His135 and His156 in *R. capsulatus*) at the Q_0 site.

Taken altogether, the docking data suggested that when cyt *b* Lys329 is substituted with Asp, the ISP-ED \sim cyt *b* complex could still form. However, the small differences seen in the fine tuning of this macromolecular recognition process (*i.e.* the rearrangement of the H-bond between residue 329 and ISP-ED His131, which in the wild type and in the cyt *b* Lys329Asp mutant involved respectively the carbonyl O and the imidazole N atom of the His) could displace the Fe_2S_2 cluster away from its optimal position in the wild type complex, decreasing the electron transfer efficiency at the Q_0 site during QH_2 catalysis.

Discussion

The photosynthetic bacteria provide a particularly suitable experimental system to study the internal redox reactions of cyt *bc*₁ during its function. These species allow assessing the activity of cyt *bc*₁ via their Ps growth ability for which cyt *bc*₁ is essential. Moreover, the catalytic core of bacterial cyt *bc*₁ is very similar to its homologs in other organisms, including mitochondria and chloroplasts of eukaryotes [54]. Thus, the metabolic flexibility and relative simplicity of bacterial systems facilitate mechanistic investigations of cyt *bc*₁, and the specific roles of the conserved amino acid residues in the electron and proton transfer reactions using site-directed mutagenesis. These attributes have been exploited extensively using the *R. capsulatus* and *R. sphaeroides* species. As the oxidation of QH_2 at the Q_0 site of cyt *bc*₁ is a critical step for the generation of a proton gradient during both Ps and Res electrons transport and ATP synthesis, the structure-function studies are important for understanding at the molecular level the physico-chemical bases of cyt *bc*₁ internal reactions.

The electron transfer steps that occur during the cyt *bc*₁ catalysis are generally well understood, and their plausible harmful consequences have been assessed [12]. However, the residues involved in proton release and uptake at the Q_0 and Q_i sites, respectively, remain less well defined [14, 5559]. Towards this aspect of cyt *bc*₁ catalysis, we examined the role(s) of several highly conserved cyt *b* residues. In particular, using EXAF spectroscopy and site-directed mutagenesis, we identified a cluster of residues located near the Q_0 site as putative participants of a proton egress pathway because of their abilities to coordinate Zn^{2+} [60]. Among them, we showed that Glu295 [56] and His291 [16] were important for proton release following QH_2 oxidation at the Q_0 site of cyt *bc*₁. In the present work, we focused on the conserved cyt *b* Lys329 residue at the cyt *b* \sim ISP-ED interaction surface. This residue is a player during the formation of the initial enzyme-substrate complex to initiate the first

electron and proton transfer during the oxidation of QH₂ by the oxidized Fe₂S₂ cluster at the Q_o site. Examination of the residues of the cyt *b* ~ ISP-ED complex docked in the *b*-position, indicated that Lys329 is one of the two residues that could be electrostatically charged under physiological conditions [17]. The three dimensional structure of *R. sphaeroides* cyt *bc*₁ showed that Lys329 formed two H-bonds with the carbonyl oxygen atoms of Thr130 and His131 of the Rieske ISP protein (PDB, 2FYN). These H-bonds are apparently critical for correct positioning of the ISP-ED on the cyt *b* surface where it docks [17]. Experimental work showed that the *R. sphaeroides* Lys329Gly (same in *R. capsulatus*) mutant slowed QH₂ oxidation, without affecting the Ps growth [26] (the growth medium was not specified). Further, the *R. sphaeroides* Lys329Ala substitution slowed by about three fold the cyt *bc*₁ activity both in membranes and purified enzyme [17]. These earlier works documented that cyt *b* Lys329 affected cyt *bc*₁ activity, but provided no information about the role, if any, of a positive charge at this position for Q_o site reactions. Interestingly, theoretical and experimental works emphasized electrostatic interactions of the anionic Fe₂S₂ clusters with a nearby positively charged residue [27]. Thus, three different *R. capsulatus* mutants carrying the Lys329Arg, Ala and Asp substitutions were obtained. The Lys329Arg had no effect on cyt *bc*₁ activity or *R. capsulatus* Ps growth, but both the Ala and Asp mutants impaired to different degrees the Ps growth and cyt *bc*₁ activity (Fig. 1) (Table 4). In the mutants, the defects were due to decreased steady-state activities and not to decreased amounts of cyt *bc*₁, in line with the decreased (33% of wild type) activity of the Ala substitution reported [17]. Comparison of the findings with the different Lys329 substitutions indicated that while losing the positive charge at position 329 of cyt *b* inhibited partly cyt *bc*₁ activity and Ps growth, and replacing it with a negative charge abolished drastically these features, providing support to the earlier described electrostatic interactions between the anionic state of the Fe₂S₂ cluster and a nearby positively charged side chain [27, 61].

The electrogenic reactions within the cyt *bc*₁, heme *b*_H reduction, and cyt *c* re-reduction kinetics examined by single flash spectroscopy confirmed the defects seen in the mutants. While no significant change was detected with the Arg substitution, the Ala and Asp induced slight and pronounced inhibition, respectively of QH₂ oxidation at the Q_o site (Figs. 4 to 7). Similarly, antimycin-sensitive CS phase III showed decreased electron transfer rates from heme *b*_H to the Q_i site, and heme *b*_H reduction kinetics in the presence of antimycin in the Ala, and especially Asp, mutants showed slower transfer of the second electron of the QH₂ oxidation to the low potential redox chain of cyt *bc*₁ (Fig. 4 and 7). Given the branched nature of QH₂ oxidation at the Q_o site, these observations could be attributed to either a direct impairment of the partial reactions of the cyt *b* chain, or a consequence of inhibition of the first electron transfer step to the high potential chain of cyt *bc*₁. Thus, the effect of the Lys329 mutations on flash-induced cyt *c* re-reduction kinetics were monitored. Different myxothiazol-sensitive cyt *c* re-reduction kinetics seen in different mutants (Fig. 6) indicated that electron transfer from the Q_o site to the high potential chain of cyt *bc*₁ occurred at different rates in different strains. Moreover, stigmatellin-induced amplitude increase of oxidized cyts *c* were seen in all cases, indicating that the large scale movement of the ISP-ED was not abolished (Figs. 6, 7B). However, in the absence of inhibitor, the cyt *c* re-reduction kinetics were dramatically slowed down in the Lys329Asp mutant, hindering QH₂

oxidation at the Q_o site. In addition, flash-induced acidification of the chromatophores lumen monitored using NR showed a markedly impaired proton release kinetics, in the case of the Lys329Asp mutant, demonstrating that proton release associated with QH_2 oxidation at the Q_o site became defective (Fig. 9).

Recently, the bifurcation of the electron transfer pathway associated with QH_2 oxidation at the Q_o site has been proposed to involve the formation of a low energy $SQ-[2Fe-2S]^+$ spin-coupled center. Generation of an $SQ-[2Fe-2S]^+$ spin-coupled center at the Q_o site of cyt bc_1 also occurs in redox-poised (by continuous illumination) photosynthetic membranes from *R. capsulatus* [11]. Based on this line of thought, a concomitant inhibition of cyt c re-reduction and cyt b_H reduction (in the presence of antimycin) in the Lys329Asp mutant could also be accounted for by inhibition of the second electron transfer (specifically to the b_L heme) along the b chain. In fact, a defect in electron transfer to the b_L heme would impede the delivery of the electron from the $SQ-[2Fe-2S]^+$ spin-coupled center to cyt c_1 . However, based on the FeS-cyt b *in silico* molecular docking data, theoretical considerations ensuing from the DFT-continuum electrostatic calculations, and considering the location of the Lys329 residue in cyt b , we propose that the replacement of a positive charge by a negative charge (Lys to Asp) interferes directly with the delivery of the first electron and proton from QH_2 at the Q_o site to the oxidized Fe_2S_2 center, affecting the distance between these two redox partners and the surrounding H-bonding patterns.

Comparative *in silico* molecular recognition (docking) calculations using the wild type and Lys329Asp mutant cyt bc_1 assessed the structural basis of the electron and proton transfer impairments induced by changing a positive charge to a negative charge at the ISP-ED ~ cyt b interface. The output from the calculations indicated a slightly energetically disfavored ISP-ED ~ cyt b surface interaction in the case of Lys329Asp as compared with the native structure, suggesting that the positively charged Lys residue stabilizes the cyt b ~ ISP-ED interface by interacting with the His ligands of the Fe_2S_2 cluster. Stabilization of the deprotonated, oxidized cluster then drives the proton transfer from QH_2 more effectively, and similarly, a negatively charged Asp residue has the opposite effect [27, 61].

Presenting the argument in greater detail, the nearby positive Lys residue from the cyt b subunit will interact with the Fe_2S_2 cluster of the ISP, which is an anion in most redox and protonation states, bearing either a 1- or 2- overall charge. In the oxidized cluster, with composition $(Cys^-)_2Fe(III)_2S_2(His)_2$, each His can be either negative (1-) deprotonated, or neutral (0) protonated. Both DFT-electrostatics calculations and redox potential measurements versus pH of the isolated ISP-ED show a similar picture. Above about pH=8, one His ligand is deprotonated (and one His is protonated) in the oxidized state until about pH>10, where both become deprotonated. By contrast, the reduced state remains protonated at both His residues until about pH=12. The corresponding pK_a 's for the two His residues of the free ISP-ED were measured as 7.5 and 9.2 in the oxidized bovine (similarly 7.8 and 9.6 in *Thermus thermophilus*), and above $pK_a=10$ in reduced bovine (similarly at $pK_a=12.5$ in *Thermus thermophilus*), consistent with DFT calculations on bovine, $pK_a=6.9$ and 8.8 for the oxidized, $pK_a=11.3$ and 12.8 for the reduced forms [27, 29, 61]. Translating these results to the full cyt bc_1 , the number of protons transferred on one-electron reduction is typically one, but this depends on the pH of the environment, and on the way the cyt b subunit shifts

the pK_a 's of the His residues in the oxidized cluster. The positively charged Lys nearby will shift the pK_a 's of one or two His residues down in the oxidized state, facilitating deprotonation of one or both sites, and acting to augment the coupled electron transfer/proton transfer capacity of the ISP-ED. The Arg mutant will have a similar effect, while the negatively charged Asp mutant will shift the pK_a 's up, stabilizing the doubly protonated oxidized state, and eliminating proton transfer from QH₂.

Another important feature to be considered is the mobility of the Lys and Arg residues side chains, seen also in other biochemical systems [62, 63]. Both are long, flexible and mobile, which can facilitate H-bonding to the His residues in the oxidized state, and movement of the positive side chain away in the reduced, doubly protonated state. These facts and predictions are consistent with the observations of active proton transfers in the native Lys329 and mutant Arg329 structures, and strong inhibition of proton transfer in the mutant Asp329 state.

Finally, the docking data suggested that the H-bond between the amino side chain of Lys329 and the carbonyl backbone oxygen of the ISP-ED residue His131 might be substituted by a H-bond between this amino side chain of Lys329 and the imidazole ring of His131. Consequently, the Fe₂S₂ cluster of ISP-ED would move away by ~ 1 Å from the Q_o site, increasing the distance between QH₂ and Fe₂S₂, and causing a decreased rate of electron transfer along the high potential electron transfer chain. A similar displacement also involves His152, which has been proposed as the direct acceptor of the first proton coupled to the first electron transfer to Fe₂S₂ [64]. Assuming an exponential decrease of the electronic coupling between QH₂ and Fe₂S₂ with distance, characterized by a decay coefficient $\beta=1.4 \text{ \AA}^{-1}$ [65], the increased QH₂-Fe₂S₂ distance would induce a four-fold decrease of the rate constant for electron transfer. This rate decrease, added to the displacement of His152 and the unfavorable deprotonation of QH₂ in the absence of a positive charge, would yield a larger inhibition to retard proton release from QH₂ and increase dramatically electron donation to Fe₂S₂ cluster [64].

In summary, the experimental data combined with the *in silico* calculations indicated that replacing a positive charge by a negative charge at position 329 of cyt *b*, which is located at the interface of ISP-ED ~ cyt *b*, affects drastically the fine docking interactions between these two subunits. Ensuing modifications of the local H-bonding patterns would move away the ISP-ED from the Q_o site and increase the distance separating QH₂ held by cyt *b* and oxidized Fe₂S₂ cluster. In addition, the absence of a positive charge nearby the oxidized Fe₂S₂ would render the deprotonation of QH₂ less efficient. Together with other similar findings [17, 25], this work shows that the precise fine control of the cyt *b* ~ ISP-ED docking interactions is essential for optimal rate of QH₂ catalysis by cyt *bc*₁. Finally, we note that multiple mutations localized in the mitochondrial cyt *b* have been shown to be responsible for severe human illness [10, 25]. The present work corroborates the idea that dissecting the cyt *bc*₁ electron transport chain, which is more easily accessible in the bacterial system, provides an invaluable tool for understanding the cause of these diseases at the molecular level, as exemplified by the study of cyt *b* Tyr278Cys mutation [66, 67].

Acknowledgments

This work was supported partly by the Division of Chemical Sciences, Geosciences and Biosciences, Office of Basic Energy Sciences of Department of Energy [DOE DE-FG02-91ER20052], and partly by the National Institute of Health [NIH GM 38237], grants to FD, and NIH grant GM 100934 to LN. FF and GV acknowledge financial support from MIUR of Italy RFO2016-17. We thank Stefan Steimle for critical reading of the manuscript, and Petru-Iulian Trasnea for help with figures. LN thanks Laura Hunsicker-Wang for valuable discussions, and Chris Putnam for early structural homology work. Some of the early ideas for this project came up in conversations with Professor James A. Fee, who will be missed.

Abbreviations:

BChl	Bacteriochlorophyll
cytochrome <i>bc</i>₁	ubiquinol:cytochrome <i>c</i> oxidoreductase
CS	carotenoid electrochromic signal
NR	Neutral Red
RC	photochemical reaction center
cyt	cytochrome
DBH₂	decylbenzohydroquinone
ISP	Iron sulfur protein
Ps	photosynthesis
Res	respiration
E_h	ambient redox potential
E_m	midpoint redox potential
Fe₂S₂ cluster	iron-sulfur cluster
Q	ubiquinone
QH₂	ubihydroquinone
Q_o	hydroquinone oxidation site
Q_i	quinone reduction site
SQ	semiquinone
R.	<i>Rhodobacter</i>

References

- [1]. Xia D, Esser L, Tang WK, Zhou F, Zhou Y, Yu L, Yu CA, Structural analysis of cytochrome *bc*₁ complexes: implications to the mechanism of function, *Biochim Biophys Acta*, 1827 (2013) 1278-1294. [PubMed: 23201476]
- [2]. Crofts AR, The Q-cycle - A Personal Perspective, *Photosynth Res*, 80 (2004) 223-243. [PubMed: 16328823]

- [3]. Schultz BE, Chan SI, Structures and proton-pumping strategies of mitochondrial respiratory enzymes, *Annu Rev Biophys Biomol Struct*, 30 (2001) 23–65. [PubMed: 11340051]
- [4]. Snyder CH, Gutierrez-Cirlos EB, Trumppower BL, Evidence for a concerted mechanism of ubiquinol oxidation by the cytochrome bc₁ complex, *J Biol Chem*, 275 (2000) 13535–13541. [PubMed: 10788468]
- [5]. Sarewicz M, Dutka M, Pintscher S, Osyczka A, Triplet state of the semiquinone-Rieske cluster as an intermediate of electronic bifurcation catalyzed by cytochrome bc₁, *Biochemistry*, 52 (2013) 6388–6395. [PubMed: 23941428]
- [6]. Pietras R, Sarewicz M, Osyczka A, Distinct properties of semiquinone species detected at the ubiquinol oxidation Qo site of cytochrome bc₁ and their mechanistic implications, *J R Soc Interface*, 13 (2016).
- [7]. Baccarini-Melandri A, Zannoni D, Photosynthetic and Respiratory Electron Flow in the Dual Functional Membrane of Facultative Photosynthetic Bacteria. *J. Bioen. Biomembr*, 10 (1978) 109–138.
- [8]. Jenney FE, Jr., Prince RC, Daldal F, Roles of the soluble cytochrome c₂ and membrane-associated cytochrome c₁ of *Rhodobacter capsulatus* in photosynthetic electron transfer, *Biochemistry*, 33 (1994) 2496–2502. [PubMed: 8117711]
- [9]. Drose S, Brandt U, The mechanism of mitochondrial superoxide production by the cytochrome bc₁ complex, *J Biol Chem*, 283 (2008) 21649–21654. [PubMed: 18522938]
- [10]. Lanciano P, Khalfaoui-Hassani B, Selamoglu N, Ghelli A, Rugolo M, Daldal F, Molecular mechanisms of superoxide production by complex III: a bacterial versus human mitochondrial comparative case study, *Biochim Biophys Acta*, 1827 (2013) 1332–1339. [PubMed: 23542447]
- [11]. Sarewicz M, Bujnowicz L, Osyczka A, Generation of semiquinone-[2Fe-2S](+) spin-coupled center at the Qo site of cytochrome bc₁ in redox-poised, illuminated photosynthetic membranes from *Rhodobacter capsulatus*, *Biochim Biophys Acta Bioenerg*, 1859 (2018) 145–153. [PubMed: 29180241]
- [12]. Osyczka A, Moser CC, Daldal F, Dutton PL, Reversible redox energy coupling in electron transfer chains, *Nature*, 427 (2004) 607–612. [PubMed: 14961113]
- [13]. Borek A, Sarewicz M, Osyczka A, Movement of the iron-sulfur head domain of cytochrome bc₁ transiently opens the catalytic Qo site for reaction with oxygen, *Biochemistry*, 47 (2008) 12365–12370. [PubMed: 18956890]
- [14]. Crofts AR, Hong S, Ugulava N, Barquera B, Gennis R, Guergova-Kuras M, Berry EA, Pathways for proton release during ubihydroquinone oxidation by the bc₁ complex, *Proc Natl Acad Sci U S A*, 96 (1999) 10021–10026. [PubMed: 10468555]
- [15]. Qu YG, Zhou F, Yu L, Yu CA, Effect of mutations of arginine 94 on proton pumping, electron transfer, and superoxide anion generation in cytochrome b of the bc₁ complex from *Rhodobacter sphaeroides*, *J Biol Chem*, 288 (2013) 1047–1054. [PubMed: 23209298]
- [16]. Francia F, Malferrari M, Lanciano P, Steimle S, Daldal F, Venturoli G, The cytochrome b Zn binding amino acid residue histidine 291 is essential for ubihydroquinone oxidation at the Qo site of bacterial cytochrome bc₁, *Biochim Biophys Acta*, 1857 (2016) 1796–1806. [PubMed: 27550309]
- [17]. Esser L, Gong X, Yang S, Yu L, Yu CA, Xia D, Surface-modulated motion switch: capture and release of iron-sulfur protein in the cytochrome bc₁ complex, *Proc Natl Acad Sci U S A*, 103 (2006) 13045–13050. [PubMed: 16924113]
- [18]. Crofts AR, Hong S, Zhang Z, Berry EA, Physicochemical aspects of the movement of the Rieske iron sulfur protein during quinol oxidation by the bc₁ complex from mitochondria and photosynthetic bacteria, *Biochemistry*, 38 (1999) 15827–15839. [PubMed: 10625447]
- [19]. Darrouzet E, Valkova-Valchanova M, Moser CC, Dutton PL, Daldal F, Uncovering the [2Fe2S] domain movement in cytochrome bc₁ and its implications for energy conversion, *Proc Natl Acad Sci U S A*, 97 (2000) 4567–4572. [PubMed: 10781061]
- [20]. Darrouzet E, Daldal F, Protein-protein interactions between cytochrome b and the Fe-S protein subunits during QH₂ oxidation and large-scale domain movement in the bc₁ complex, *Biochemistry*, 42 (2003) 1499–1507. [PubMed: 12578362]

- [21]. Tian H, White S, Yu L, Yu CA, Evidence for the head domain movement of the rieske iron-sulfur protein in electron transfer reaction of the cytochrome bc₁ complex, *J Biol Chem*, 274 (1999) 7146–7152. [PubMed: 10066773]
- [22]. Xiao K, Yu L, Yu CA, Confirmation of the involvement of protein domain movement during the catalytic cycle of the cytochrome bc₁ complex by the formation of an intersubunit disulfide bond between cytochrome b and the iron-sulfur protein, *J Biol Chem*, 275 (2000) 38597–38604. [PubMed: 10978350]
- [23]. Darrouzet E, Daldal F, Movement of the iron-sulfur subunit beyond the ef loop of cytochrome b is required for multiple turnovers of the bc₁ complex but not for single turnover Q_O site catalysis, *J Biol Chem*, 277 (2002) 3471–3476. [PubMed: 11707449]
- [24]. Xiao K, Engstrom G, Rajagukguk S, Yu CA, Yu L, Durham B, Millett F, Effect of famoxadone on photoinduced electron transfer between the iron-sulfur center and cytochrome c₁ in the cytochrome bc₁ complex, *J Biol Chem*, 278 (2003) 11419–11426. [PubMed: 12525495]
- [25]. Ekiert R, Borek A, Kuleta P, Czernek J, Osyczka A, Mitochondrial disease-related mutations at the cytochrome b-iron-sulfur protein (ISP) interface: Molecular effects on the large-scale motion of ISP and superoxide generation studied in *Rhodobacter capsulatus* cytochrome bc₁, *Biochim Biophys Acta*, 1857 (2016) 1102–1110. [PubMed: 27032290]
- [26]. Crofts AR, Barquera B, Bechmann G, Guergova M, Salcedo-Hernandez R, Hacker B, Hong S, Gennis RB, Structure and Function in the bc₁-complex of *Rhodobacter sphaeroides* Kluwer Academic Publishers, Place Published, 1995.
- [27]. Ullmann GM, Noodleman L, Case DA, Density functional calculation of p K(a) values and redox potentials in the bovine Rieske iron-sulfur protein, *J Biol Inorg Chem*, 7 (2002) 632–639. [PubMed: 12072969]
- [28]. Zu Y, Fee JA, Hirst J, Complete thermodynamic characterization of reduction and protonation of the bc(1)-type Rieske [2Fe-2S] center of *Thermus thermophilus*, *J Am Chem Soc*, 123 (2001) 9906–9907. [PubMed: 11583559]
- [29]. Klingen AR, Ullmann GM, Negatively charged residues and hydrogen bonds tune the ligand histidine pKa values of Rieske iron-sulfur proteins, *Biochemistry*, 43 (2004) 12383–12389. [PubMed: 15449929]
- [30]. Davidson E, Ohnishi T, Tokito M, Daldal F, *Rhodobacter capsulatus* mutants lacking the Rieske FeS protein form a stable cytochrome bc₁ subcomplex with an intact quinone reduction site, *Biochemistry*, 31 (1992) 3351–3358. [PubMed: 1313293]
- [31]. Gray KA, Davidson E, Daldal F, Mutagenesis of methionine-183 drastically affects the physicochemical properties of cytochrome c₁ of the bc₁ complex of *Rhodobacter capsulatus*, *Biochemistry*, 31 (1992) 11864–11873. [PubMed: 1332776]
- [32]. Sambrook J, Russell DW, *Molecular Cloning A Laboratory Manual*, Cold Spring Harbor Press, Place Published, 2001.
- [33]. Lanciano P, Lee DW, Yang H, Darrouzet E, Daldal F, Intermonomer electron transfer between the low-potential b hemes of cytochrome bc(1), *Biochemistry*, 50 (2011) 1651–1663. [PubMed: 21261281]
- [34]. Khalfoui-Hassani B, Lanciano P, Daldal F, A robust genetic system for producing heterodimeric native and mutant cytochrome bc(1), *Biochemistry*, 52 (2013) 7184–7195. [PubMed: 24028512]
- [35]. Atta-Asafo-Adjei E, Daldal F, Size of the amino acid side chain at position 158 of cytochrome b is critical for an active cytochrome bc₁ complex and for photosynthetic growth of *Rhodobacter capsulatus*, *Proc Natl Acad Sci U S A*, 88 (1991) 492–496. [PubMed: 1846443]
- [36]. Baccarini-Melandri A, Melandri AB, Partial Resolution of Phosphorylating system of *Rps. capsulata*, *Methods Enzymol.*, 23 (1971) 556–561.
- [37]. Mulkidjanian AY, Junge W, Calibration and time resolution of luminal pH-transients in chromatophores of *Rhodobacter capsulatus* following a single turnover flash of light: proton release by the cytochrome bc₁-complex is strongly electrogenic, *FEBS Lett*, 353 (1994) 189–193. [PubMed: 7926049]
- [38]. Clatyton RK, Spectroscopic Analysis of Bacteriochlorophylls in vivo and in vitro, *Photochem. Photobiol* 5 (1963) 669–677.

- [39]. Esser L, Elberry M, Zhou F, Yu CA, Yu L, Xia D, Inhibitor-complexed structures of the cytochrome bc₁ from the photosynthetic bacterium *Rhodobacter sphaeroides*, *J Biol Chem*, 283 (2008) 2846–2857. [PubMed: 18039651]
- [40]. Dominguez C, Boelens R, Bonvin AM, HADDOCK: a protein-protein docking approach based on biochemical or biophysical information, *J Am Chem Soc*, 125 (2003) 1731–1737. [PubMed: 12580598]
- [41]. van Zundert GCP, Rodrigues J, Trellet M, Schmitz C, Kastiris PL, Karaca E, Melquiond ASJ, van Dijk M, de Vries SJ, Bonvin A, The HADDOCK2.2 Web Server: User-Friendly Integrative Modeling of Biomolecular Complexes, *J Mol Biol*, 428 (2016) 720–725. [PubMed: 26410586]
- [42]. Ashkenazy H, Abadi S, Martz E, Chay O, Mayrose I, Pupko T, Ben-Tal N, ConSurf 2016: an improved methodology to estimate and visualize evolutionary conservation in macromolecules, *Nucleic Acids Res*, 44 (2016) W344–350. [PubMed: 27166375]
- [43]. Sali A, Blundell TL, Comparative protein modelling by satisfaction of spatial restraints, *J Mol Biol*, 234 (1993) 779–815. [PubMed: 8254673]
- [44]. Webb B, Sali A, Comparative Protein Structure Modeling Using MODELLER, *Curr Protoc Bioinformatics*, 54 (2016) 561–5637.
- [45]. Schuttelkopf AW, van Aalten DM, PRODRG: a tool for high-throughput crystallography of protein-ligand complexes, *Acta Crystallogr D Biol Crystallogr*, 60 (2004) 1355–1363. [PubMed: 15272157]
- [46]. Valiev M, Blaska EJ, Govind N, Kowaski K, Straatsma TP, Van Dam HJJ, Wang D, Nieplocha J, Apra E, Windus TL, de Jong WA, NWChem: A Comprehensive and Scalable Open Source Solution for Large Scale Molecular Simulations., *Comp. Phys. Comm*, 181 (2010) 1477–1489.
- [47]. Pettersen EF, Goddard TD, Huang CC, Couch GS, Greenblatt DM, Meng EC, Ferrin TE, UCSF Chimera—a visualization system for exploratory research and analysis, *J Comput Chem*, 25 (2004) 1605–1612. [PubMed: 15264254]
- [48]. Hochkoeppler A, Jenney FE, Jr., Lang SE, Zannoni D, Daldal F, Membrane-associated cytochrome cy of *Rhodobacter capsulatus* is an electron carrier from the cytochrome bc₁ complex to the cytochrome c oxidase during respiration, *J Bacteriol*, 177 (1995) 608–613. [PubMed: 7836293]
- [49]. Jackson JB, Dutton PL, The kinetic and redox potentiometric resolution of the carotenoid shifts in *Rhodospseudomonas spheroides* chromatophores: their relationship to electric field alterations in electron transport and energy coupling, *Biochim Biophys Acta*, 325 (1973) 102–113. [PubMed: 4358810]
- [50]. Crofts AR, Wood PM, Photosynthetic Electron Transport Chains of Plants and Bacteria and their Role in Proton Pumps, *Curr. Top. Bioenerg* 7 (1978) 175–244.
- [51]. Glaser EG, Crofts AR, A new electrogenic step in the ubiquinol:cytochrome c₂ oxidoreductase complex of *Rhodospseudomonas sphaeroides*, *Biochim Biophys Acta*, 766 (1984) 322–333. [PubMed: 6087897]
- [52]. Mulikidjanian AY, Activated Q-cycle as a common mechanism for cytochrome bc₁ and cytochrome b₆f complexes, *Biochim Biophys Acta*, 1797 (2010) 1858–1868. [PubMed: 20650262]
- [53]. Berry EA, Huang LS, Saechao LK, Pon NG, Valkova-Valchanova M, Daldal F, X-Ray Structure of *Rhodobacter capsulatus* cytochrome bc₁: Comparison with its Mitochondrial and Chloroplast Counterparts, *Photosynth Res*, 81 (2004) 251–275. [PubMed: 16034531]
- [54]. Darrouzet E, Cooley JW, Daldal F, The Cytochrome bc₁ Complex and its Homologue the b₆f Complex: Similarities and Differences, *Photosynth Res*, 79 (2004) 25–44. [PubMed: 16228398]
- [55]. Osyczka A, Zhang H, Mathe C, Rich PR, Moser CC, Dutton PL, Role of the PEWY glutamate in hydroquinone-quinone oxidation-reduction catalysis in the Qo Site of cytochrome bc₁, *Biochemistry*, 45 (2006) 10492–10503. [PubMed: 16939201]
- [56]. Lee DW, El Khoury Y, Francia F, Zambelli B, Ciurli S, Venturoli G, Hellwig P, Daldal F, Zinc inhibition of bacterial cytochrome bc₁ reveals the role of cytochrome b E295 in proton release at the Q(o) site, *Biochemistry*, 50 (2011) 4263–4272. [PubMed: 21500804]

- [57]. Postila PA, Kaszuba K, Sarewicz M, Osyczka A, Vattulainen I, Rog T, Key role of water in proton transfer at the Q_o-site of the cytochrome bc₁ complex predicted by atomistic molecular dynamics simulations, *Biochim Biophys Acta*, 1827 (2013) 761–768. [PubMed: 23428399]
- [58]. Wilson CA, Crofts AR, Dissecting the pattern of proton release from partial process involved in ubihydroquinone oxidation in the Q-cycle, *Biochim Biophys Acta*, 1859 (2018) 531–543.
- [59]. Kuleta P, Sarewicz M, Postila P, Rog T, Osyczka A, Identifying involvement of Lys251/Asp252 pair in electron transfer and associated proton transfer at the quinone reduction site of *Rhodobacter capsulatus* cytochrome bc₁, *Biochim Biophys Acta*, 1857 (2016) 1661–1668. [PubMed: 27421232]
- [60]. Giachini L, Francia F, Veronesi G, Lee DW, Daldal F, Huang LS, Berry EA, Cocco T, Papa S, Boscherini F, Venturoli G, X-Ray absorption studies of Zn²⁺ binding sites in bacterial, avian, and bovine cytochrome bc₁ complexes, *Biophys J*, 93 (2007) 2934–2951. [PubMed: 17573435]
- [61]. Zu Y, Couture MM, Kolling DR, Crofts AR, Eltis LD, Fee JA, Hirst J, Reduction potentials of Rieske clusters: importance of the coupling between oxidation state and histidine protonation state, *Biochemistry*, 42 (2003) 12400–12408. [PubMed: 14567701]
- [62]. Bhawe DP, Han WG, Pazicni S, Penner-Hahn JE, Carroll KS, Noodleman L, Geometric and electrostatic study of the [4Fe4S] cluster of adenosine-5'-phosphosulfate reductase from broken symmetry density functional calculations and extended X-ray absorption fine structure spectroscopy, *Inor. Chem*, 50 (2011) 6610–6625.
- [63]. Asthagiri D, Dillet V, Liu T, Noodleman L, Van Etten RL, Bashford D, Density functional study of the mechanism of a tyrosine phosphatase: I. Intermediate formation., *J Am Chem Soc*, 124 (2002) 10225–10235. [PubMed: 12188687]
- [64]. Crofts AR, Hong S, Wilson C, Burton R, Victoria D, Harrison C, Schulten K, The mechanism of ubihydroquinone oxidation at the Q_o site of the cytochrome bc₁ complex, *Biochim Biophys Acta*, 1827 (2013) 1362–1377. [PubMed: 23396004]
- [65]. Moser CC, Keske JM, Warncke K, Farid RS, Dutton PL, Nature of biological electron transfer, *Nature*, 355 (1992) 796–802. [PubMed: 1311417]
- [66]. Lee DW, Selamoglu N, Lanciano P, Cooley JW, Forquer I, Kramer DM, Daldal F, Loss of a conserved tyrosine residue of cytochrome b induces reactive oxygen species production by cytochrome bc₁, *J Biol Chem*, 286 (2011) 18139–18148. [PubMed: 21454570]
- [67]. Ghelli A, Tropeano CV, Calvaruso MA, Marchesini A, Iommarini L, Porcelli AM, Zanna C, De Nardo V, Martinuzzi A, Wibrand F, Vissing J, Kurelac I, Gasparre G, Selamoglu N, Daldal F, Rugolo M, The cytochrome b p.278Y>C mutation causative of a multisystem disorder enhances superoxide production and alters supramolecular interactions of respiratory chain complexes, *Hum Mol Genet*, 22 (2013) 2141–2151. [PubMed: 23418307]
- [68]. Ditta G, Schmidhauser T, Yakobson E, Lu P, Liang XW, Finlay DR, Guiney D, Helinski DR, Plasmids related to the broad host range vector, pRK290, useful for gene cloning and for monitoring gene expression, *Plasmid*, 13 (1985) 149–153. [PubMed: 2987994]

Highlights

- The cyt *b* Lys329 of cyt *bc*₁ was substituted by other amino acids
- Among the mutants the Lys329Asp was incapable of cyt *bc*₁-dependent growth
- Lys329 substitutions did not affect the cofactors or assembly of cyt *bc*₁
- Lys329Asp mutant inhibited drastically Q_o site catalysis in chromatophores
- Lys329Asp could modify H-bonding network around the Fe₂S₂ cluster at the Q_o site
- A positive charge at cyt *b* 329 is required for QH₂ oxidation

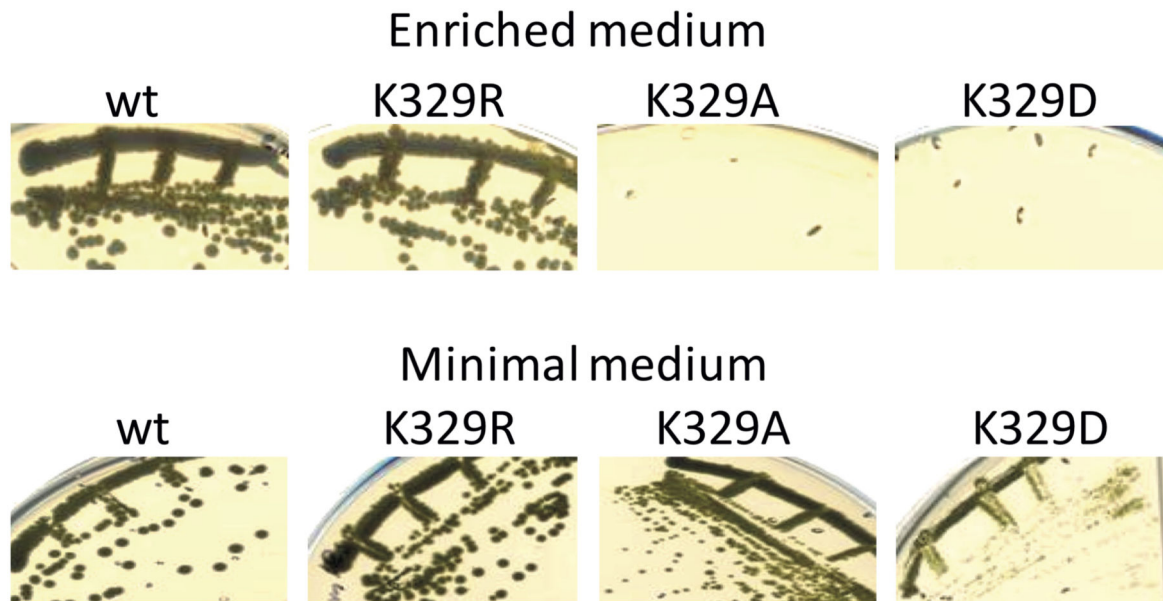


Figure 1. Photosynthetic growth phenotype of *cyt b* Lys329 mutants.

R. capsulatus wild type (wt), Lys329Arg (K329R), Lys329Ala (K329A), and Lys329Asp (K329D) strains grown by photosynthesis on agar plates containing enriched (unbuffered) or minimal (buffered) media. Ps growth defects of Ala and Asp substitutions are more severe in the former medium. All strains are proficient for aerobic respiratory growth in both media (data not shown).

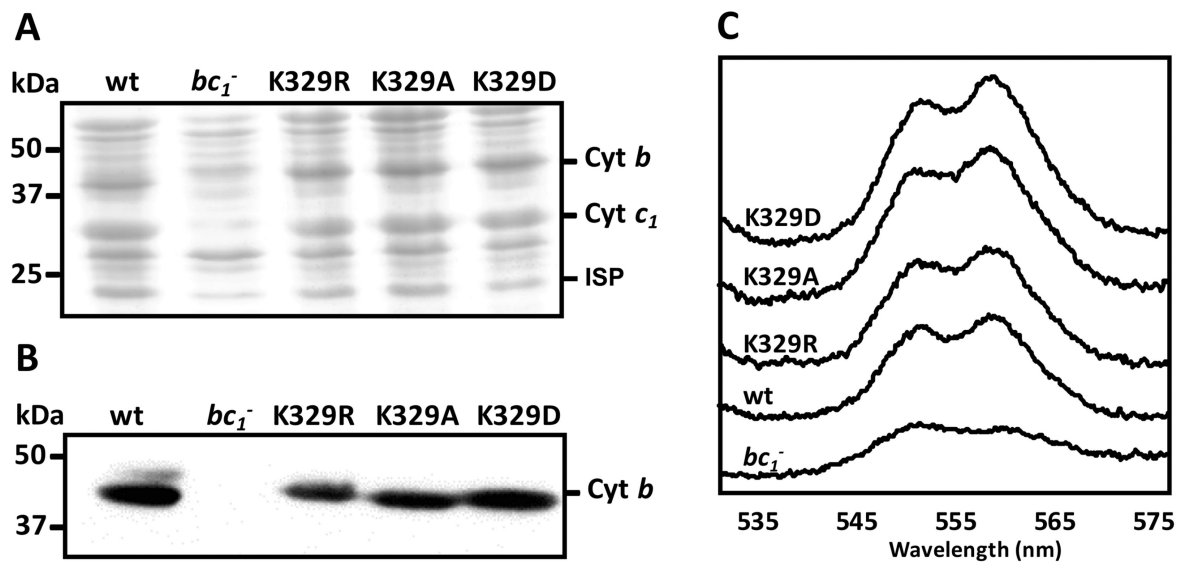


Figure 2. Properties of *R. capsulatus* strains producing *cyt b* Lys329 mutants.

A- SDS-PAGE (for *cyt b* and *cyt c*₁) and **B-** immunoblot analyses (for *cyt b*) of *cyt bc*₁ subunits in strains carrying the *cyt b* Lys329 mutants. Chromatophore membranes (40 μg of total proteins) from wild type (wt), *cyt bc*₁-minus mutant (*bc*₁⁻), Lys329Arg (K329R), Lys329Ala (K329A) and Lys329Asp (K329D) mutants were probed with polyclonal anti-*cyt b* (Materials and Methods). **C-** Optical redox difference spectra of chromatophore membranes of the same strains as in B. The absorption difference spectra were recorded between 530 and 580 nm using ferricyanide-oxidized membrane preparations as a baseline and reducing the sample with excess of sodium dithionite.

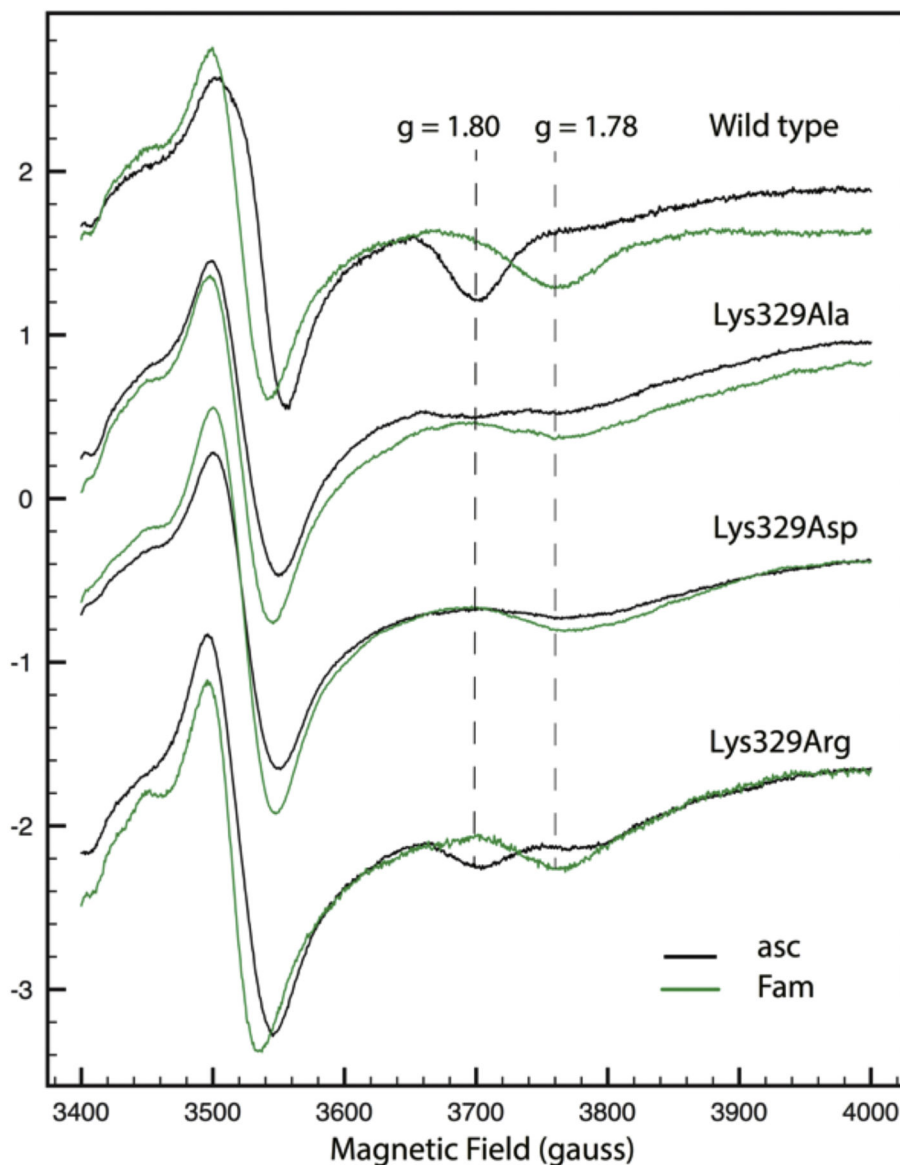


Figure 3. EPR characterization of *R. capsulatus* strains carrying the *cyt b* Lys329Ala, Asp or Arg substitutions. EPR spectra of membranes prepared from wild type (pMTS1/MT-RBC1) *Rhodobacter capsulatus* strain and its *cyt b* Lys329Ala, Lys329Asp and Lys329Arg mutant derivatives, as described in Materials and Methods, and reduced with ascorbate (asc) in the absence (black traces) and presence (green traces) of famoxadone (Fam). The g_x EPR transitions (g values of 1.8 and 1.78) corresponding to the reduced Fe_2S_2 cluster of the ISP subunit of *cyt bc*₁ in the absence and presence of the inhibitor famoxadone are indicated by vertical dashed lines. The EPR spectra recording conditions were for all samples: Temperature, 20K; microwave power, 2mW at 9.4GHz; modulation amplitude 10 G at 100 kHz and four scans.

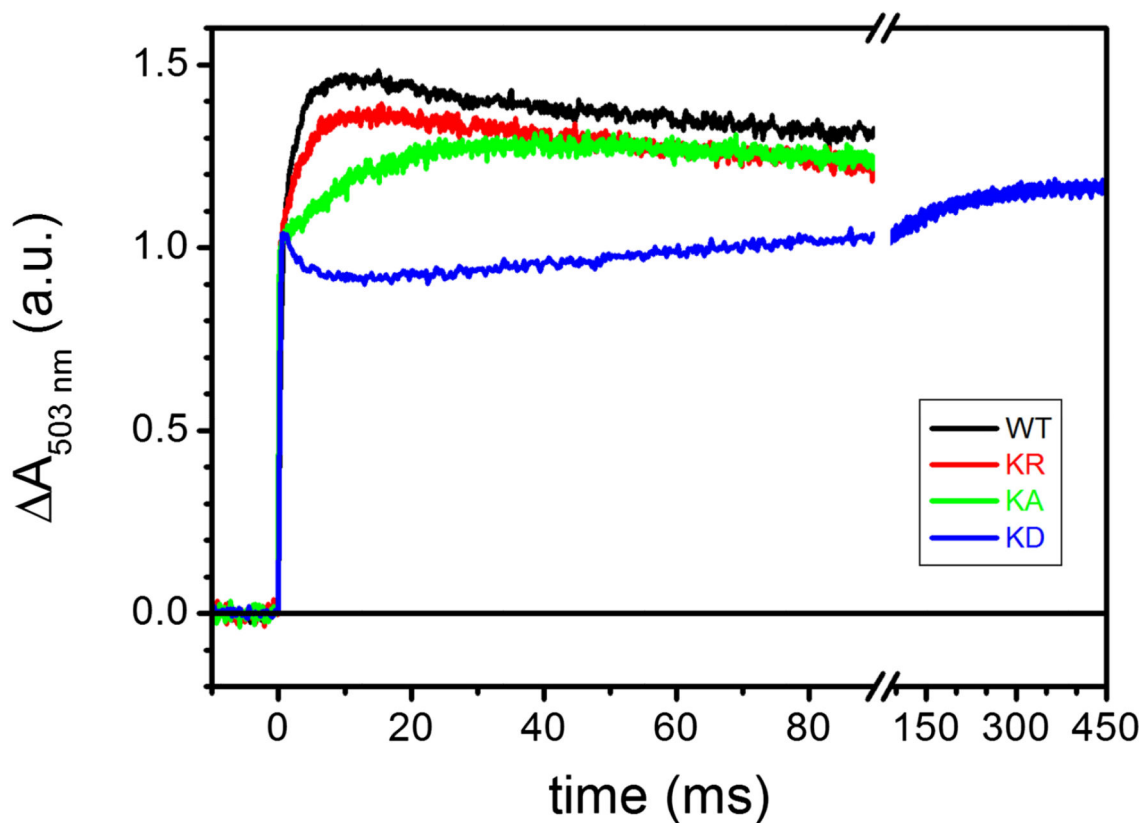


Figure 4. The effect of K329 mutations on the carotenoid electrochromic signal following a single-turnover flash.

Kinetic traces are the average of 8 events recorded at 503 nm in uninhibited chromatophores, normalized to the maximal absorption changes observed in the presence of 2 μM myxothiazol / 10 μM antimycin (see text for details). Black, WT; red, K329R; green, K329A; blue, K329D. Chromatophores at $\sim 35 \mu\text{M}$ total [BChl] were suspended in 50 mM MOPS buffer, pH 7.00, 100 mM KCl in a closed, stirred cuvette under nitrogen flow; the ambient redox potential was maintained at $115 \pm 5 \text{ mV}$ by small additions of Na-Ascorbate or K-ferrocyanide. 8 μM each of *para*-benzoquinone (*p*BQ), 1,4-naphthaquinone (1.4NQ) and 1,2-naphthaquinone (1.2NQ) were added as redox mediators.

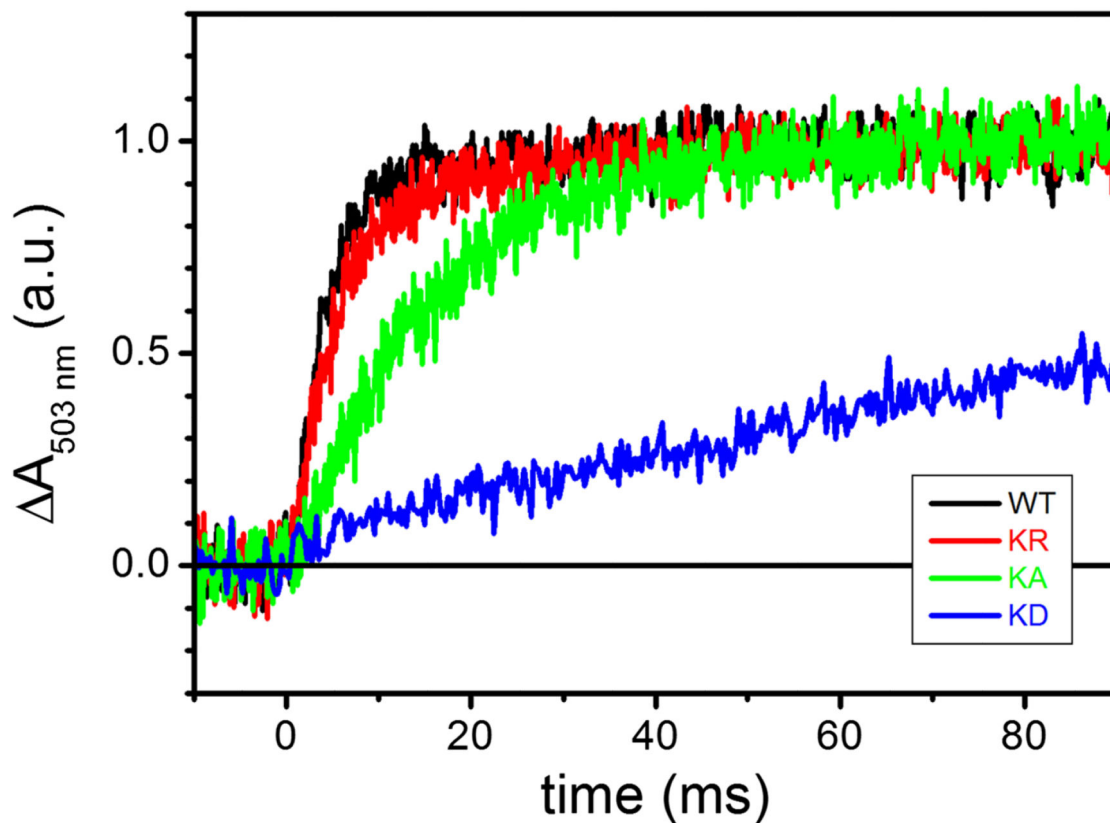


Figure 5. The effect of K329 mutations on the kinetics of the antimycin-sensitive carotenoid shift phase III.

Signals recorded in the presence of 10 μM antimycin have been subtracted from those detected in uninhibited chromatophores (see Figure 3). The obtained difference traces have been normalized to the maximal amplitude reached. Other experimental conditions are detailed in the legend of Figure 3. Black, WT; red, K329R; green, K329A; blue, K329D.

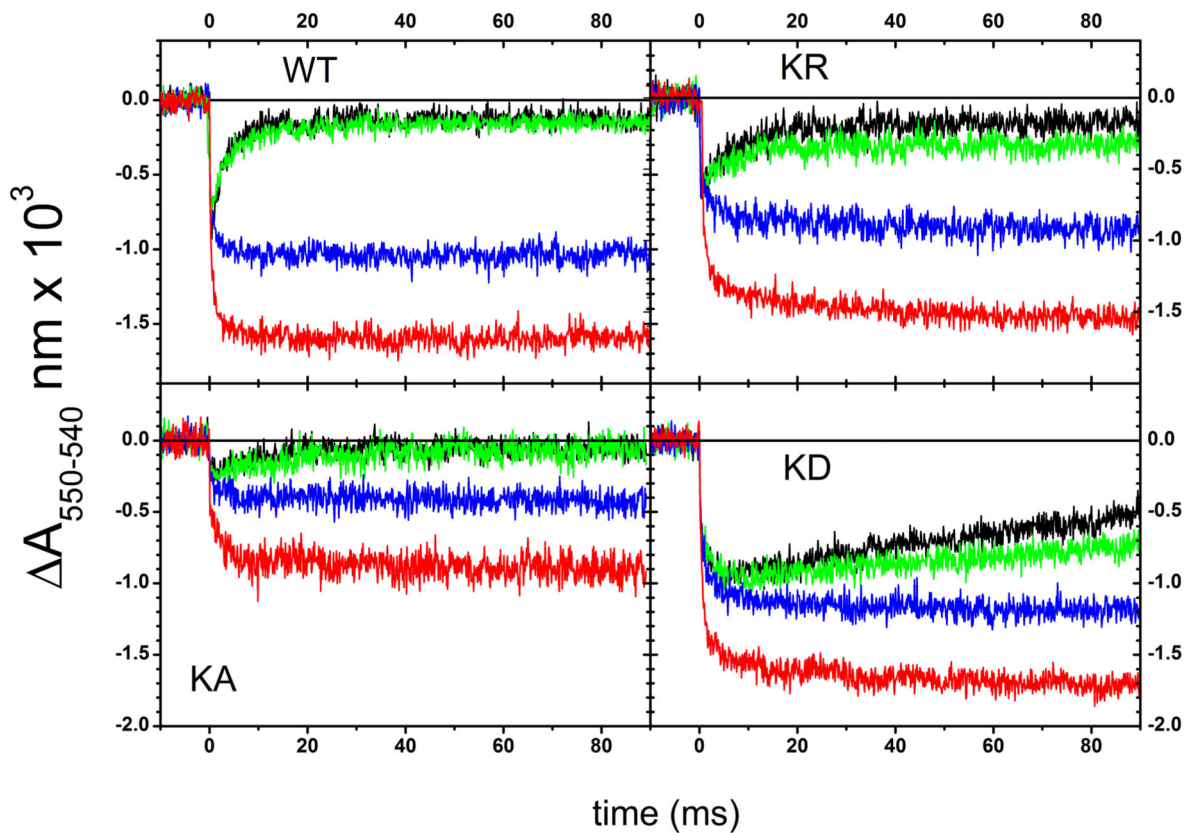


Figure 6. Kinetics of cyt *c* redox changes following a single turnover flash.

Kinetic traces recorded in uninhibited chromatophores (black), in the presence of 10 μM antimycin (green), of 10 μM antimycin and 2 μM myxothiazol (blue), and of 1 μM stigmatellin (red) are shown. The strains are indicated in the panels. Each signal is the average of 25 single events. Other experimental conditions are as described in the legend of Figure 3, except that K329A chromatophores were suspended at $\sim 25 \mu\text{M}$ [BChl], rather than $\sim 35 \mu\text{M}$ [BChl] of the other strains. Note that in this figure the colors correspond to the different kinds of inhibitors used.

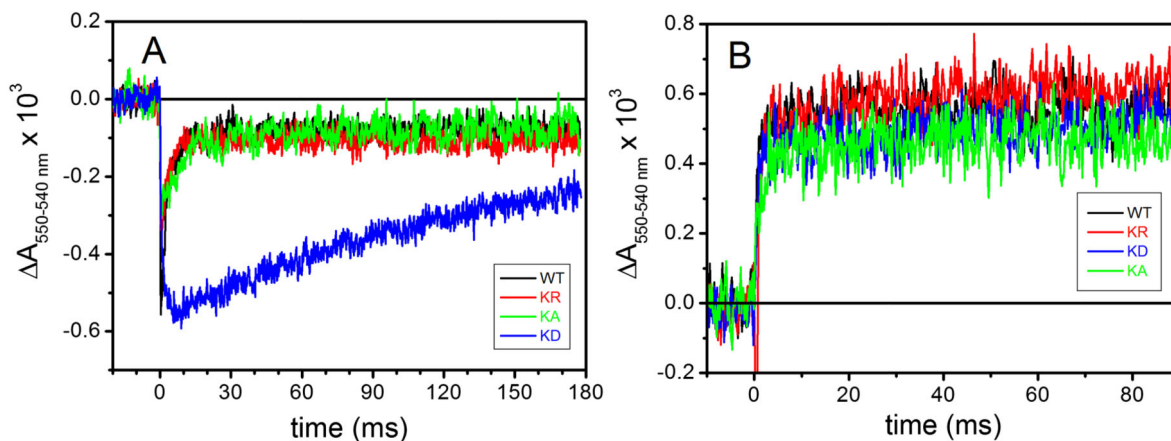


Figure 7. The effect of K329 mutations on cyt *c* kinetics.

A- cyt *c* reduction kinetics after a single flash, recorded in uninhibited chromatophores, normalized to the total extent of cyt *c* oxidation detected in the presence of 1 μ M stigmatellin. Except for normalization, the traces are the same plotted in Figure 5, but they have been shown over a longer time scale. **B-** Kinetic traces obtained by subtracting cyt *c* kinetics in the presence of stigmatellin from those recorded in the presence of antimycin/myxothiazol (blue-red traces from Figure 5). Experimental conditions as in Figure 5, color code as in figure 4.

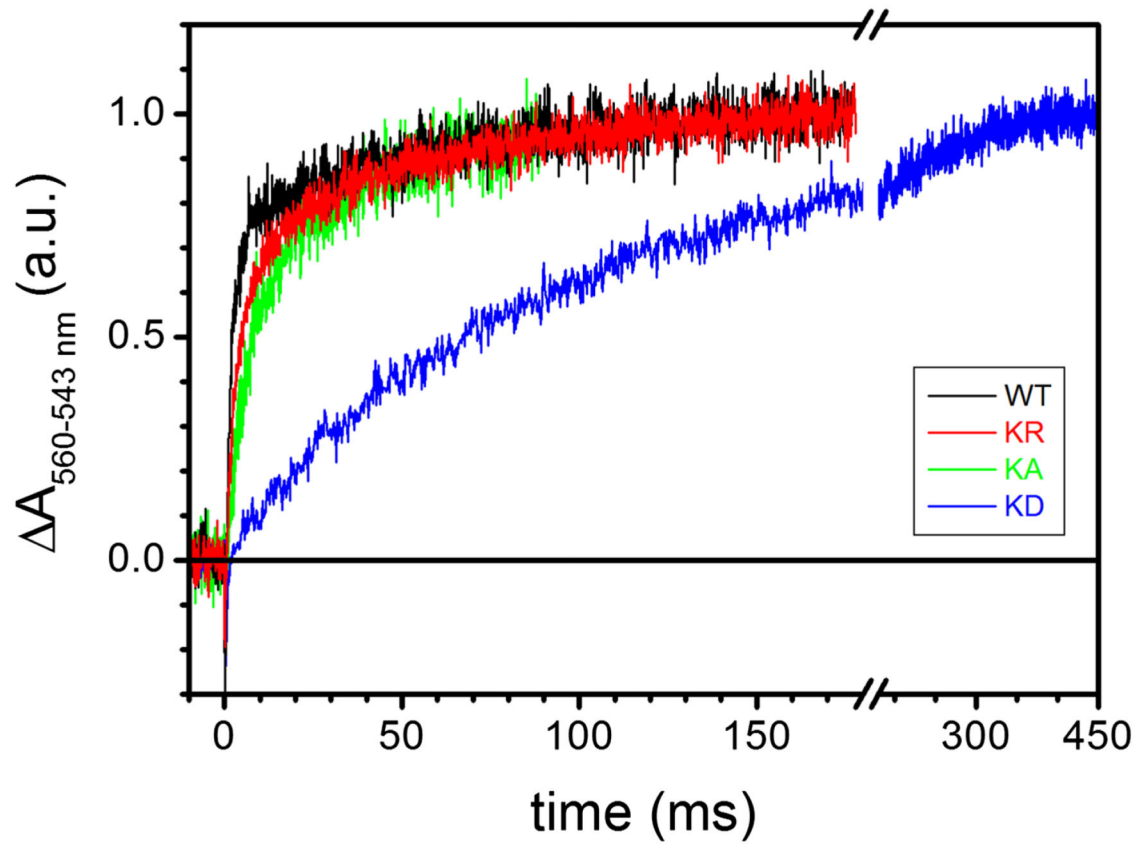


Figure 8. The effect of K329 mutations on the kinetics of heme b_H reduction following a single flash.

Traces (average of 30 single events) were recorded in the presence of 10 μM antimycin, and normalized to the maximal extent of the absorption changes. Black, WT; red, K329R; green, K329A; blue, K329D. The experimental conditions are described in the legend of Figure 3.

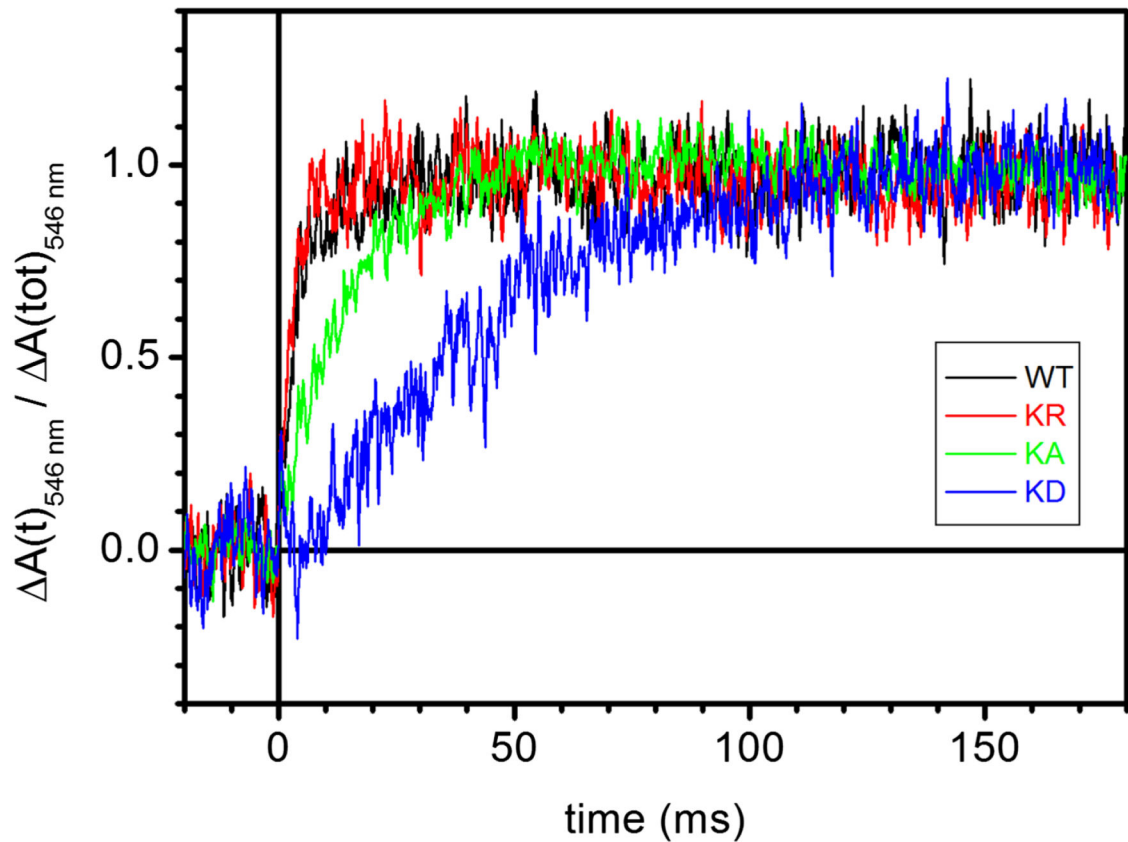


Figure 9. Neutral Red detection of flash induced acidification of the chromatophore lumen. Kinetic traces show the difference between flash-induced absorbance changes at 546 nm recorded before and after inhibition of the *bc*₁ with 10 μ M antimycin and 2 μ M myxothiazol. Chromatophores were suspended in 2 mg/mL BSA buffer, pH 7.5, 50 mM KCl, 13 μ M Neutral Red, 10 μ M DAD, 10 μ M oligomycin, 10 μ M valinomycin, 1 mM Na-ascorbate, 1 mM KCN in a closed, unstirred cuvette. Traces (average of 60 single events) were normalized to the stationary, maximal absorbance change, ΔA , reached. Black, WT; red, K329R; green, K329A; blue, K329D.

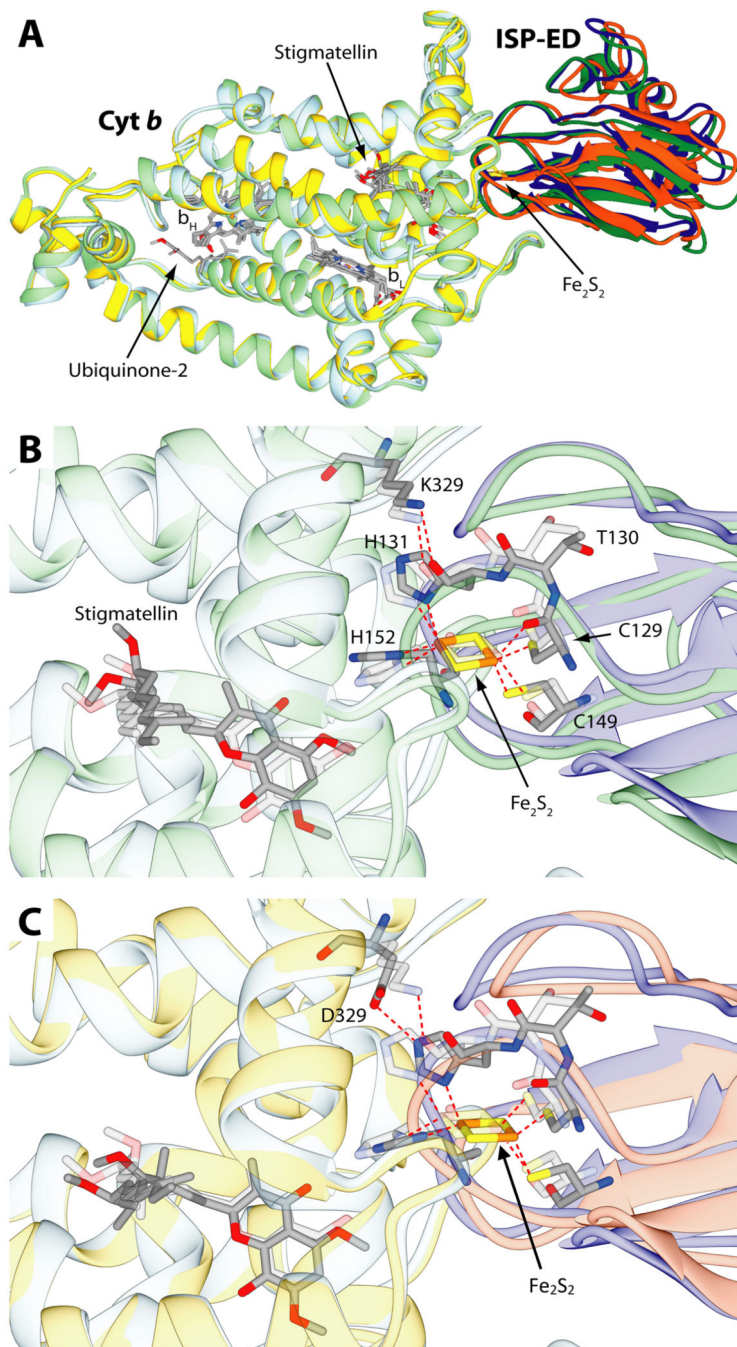


Figure 10.

Results of the docking calculations performed on *cyt b* and ISP-ED from *R. sphaeroides* and comparison with the starting crystal structure (PDB code: 2QJY). **A**- Ribbon representation of *cyt b* and ISP-ED from the crystal structure colored in light blue and blue, respectively superimposed to the result of the docking calculations in the case of the wild-type *cyt b* (light green and green) and the K329D mutant (yellow and orange). The *cyt b* ~ ISP-ED complexes were superimposed through the optimal match of the position of the *cyt b* Ca. The heme groups together with the Fe_2S_2 cluster and the ubiquinone and stigmatellin

ligands are shown as sticks colored accordingly to the atom type. (**B** and **C**)- Detail of the *cyt b* ~ ISP-ED complex, with **B**, comparing computer simulated wild type structure and **C**, computer simulated mutant structure to the wild type crystal structure, respectively. Ribbons are colored as in panel **A** and were made partially transparent for clarity. Residues and ligands cited in the text are reported as sticks colored according to the atom type. Residues from the crystal structure were also made transparent for clarity. S-Fe, N-Fe and hydrogen bonds are reported as dashed red lines.

Author Manuscript

Author Manuscript

Author Manuscript

Author Manuscript

Table 1.

Strains and Plasmids

Plasmids or strains	Description	Antibiotic Resistance	Reference
<i>Strains</i>			
E. coli			
HB101	F ⁻ (<i>gpt-proA</i>)62 <i>leuB6supE44 ara-14 galK2 lacY1 (mcrC-mrr) rpsL20</i> (Str ^R) <i>xyl-5 mtl-1recA13</i>	Str ^R	Promega
<i>R. capsulatus</i>			
MT-RBC1	<i>R. capsulatus</i> MT1131 carrying deletion on <i>petABC</i> operon (<i>petABC::spe</i>)	Spe ^R	[35]
<i>Plasmids</i>			
pRK2013	Conjugation Helper	Km ^R	[68]
pPET1-F	3.4 kb fragment of <i>petABC</i> operon in pBBR-derivative, <i>petB</i> is <i>petB-Flag</i>	Amp ^R	[33]
pMTS1	3.4 kb fragment of <i>petABC</i> operon in pRK415-derivative	Km ^R	[33]
pBK13	pPETI-F derivative carrying <i>petB::K329R</i>	Amp ^R	This work
pBK14	pPETI-F derivative carrying <i>petB::K329D</i>	Amp ^R	This work
pBK15	pPETI-F derivative carrying <i>petB::K329A</i>	Amp ^R	This work
pBK23	pMTS1 derivative carrying <i>petB::K329R</i>	Km ^R	This work
pBK29	pMTS1 derivative carrying <i>petB::K329D</i>	Km ^R	This work
pBK30	pMTS1 derivative carrying <i>petB::K329A</i>	Km ^R	This work

Table 2.Oligonucleotide primers used to generate *cyt b* Lys329 mutations

Primers	Sequence from 5' to 3'
K329R-For	GCATCGTCGATGCGAGGTTCTTCGGCGTGAT
K329R-Rev	ATCACGCCGAAGAACCTCGCATCGACGATGC
K329D-For	CGGCATCGTCGATGCGGATTCTTCGGCGTGATCG
K329D-Rev	CGATCACGCCGAAGAAATCCGCATCGACGATGCCG
K329A-For	CGGCATCGTCGATGCGGGCTTCTTCGGCGTGATC
K329A-Rev	GATCACGCCGAAGAACGCCGCATCGACGATGCCG

Author Manuscript

Author Manuscript

Author Manuscript

Author Manuscript

Table 3.

Active and passive residues used to guide the docking calculations.

Protein	Active residues	Passive residues
Cyt <i>b</i>	Trp157, Thr160, Val161, Gly164, Leu165, Thr288, Pro289, Ile292, Tyr302, Leu305, Arg306, Lys(Asp)329, Gly332, and Val333	Phe156, Gly167, Ala168, Gln177, Leu181, Val186, Pro285, Leu286, Arg287, Ala290, His291, Val293, Thr309, Ala310, Asp327, Ala328, Phe330, Ala382, Gln383, Gln384, Thr385, and Ser393
ISP-ED	Thr130, His131, Leu132, Gly133, Cys134, Cys151, His152, and Pro166	Pro71, Val128, Cys129, Ser135, Pro150, Gly153, Ile162, Gly165, Ala167, Pro168, Glu169, and Pro172

Author Manuscript

Author Manuscript

Author Manuscript

Author Manuscript

Table 4.Steady-state cyt *bc*₁ activities in various *R. capsulatus* cyt *b* Lys329 mutants

Strains	Ps growth on enriched medium	DBH ₂ activity (%)	DBH ₂ activity (%) + Ant
MT-RBC1	-	1.9 ± 0.74	ND
MT-RBC1/pMTS1 (wild type)	+	100.0 ± 4.9	13.5 ± 1.0
MT-RBC1/pBK23 (Lys329Arg)	+	85.0 ± 8.0	11.8 ± 1.3
MT-RBC1/pBK30 (Lys329Ala)	-	33.0 ± 5.3	7.2 ± 0.8
MT-RBC1/pBK29 (Lys329Asp)	-	10.7 ± 0.7	6.2

Ps growth refers to photosynthetic growth, and + or - indicates growth or no growth ability. DBH₂ activity is indicated as a % of wild type (wt) cyt *bc*₁ activity in *R. capsulatus* membranes. In this case, the 100 % of wild type activity corresponded to 1.19 μmoles of cyt *c* reduced/min/mg of total membrane proteins. The 1.9 % of wild type activity seen in MT-RBC1 lacking cyt *bc*₁ corresponds to a cyt *bc*₁-independent background activity. Ant, Antimycin A. ND, not determined. The fraction, if any, of residual antimycin-insensitive activities correspond to superoxide production was not determined.